

Research Articles: Cellular/Molecular

CLC anion/proton exchangers regulate secretory vesicle filling and granule exocytosis in chromaffin cells

<https://doi.org/10.1523/JNEUROSCI.2439-21.2022>

Cite as: J. Neurosci 2022; 10.1523/JNEUROSCI.2439-21.2022

Received: 13 December 2021

Revised: 2 February 2022

Accepted: 7 February 2022

This Early Release article has been peer-reviewed and accepted, but has not been through the composition and copyediting processes. The final version may differ slightly in style or formatting and will contain links to any extended data.

Alerts: Sign up at www.jneurosci.org/alerts to receive customized email alerts when the fully formatted version of this article is published.

CLC anion/proton exchangers regulate secretory vesicle filling and granule exocytosis in chromaffin cells

Abbreviated title: Functional role of CLC-3 in neurosecretion

Authors: Maddalena Comini^{1¶}, Juan Sierra-Marquez^{1¶}, Gustavo A. Guzman², Arne Franzen¹, Antje Willuweit³, Istvan Katona⁴, Patricia Hidalgo¹, Christoph Fahlke¹, Raul E. Guzman^{1,§}

Affiliations:

¹Institute of Biological Information Processing, Molekular- und Zellphysiologie (IBI-1), Forschungszentrum Jülich, 52428, Jülich, Germany

²Institute of Neuroscience and Medicine (INM-10), Forschungszentrum Jülich, 52428, Jülich, Germany.

³Institute of Neuroscience and Medicine (INM-4), Medical Imaging Physics, Forschungszentrum Jülich, 52428, Jülich, Germany.

⁴Institute of Neuropathology, RWTH Aachen University, Aachen, Germany

[¶]These authors contributed equally to this work

[¶] Present address: Nuffield Department of Clinical Neurosciences, University of Oxford, Oxford, OX3 9DU, UK

Corresponding author:

[§]Correspondence and requests material should be addressed to Raul E. Guzman Email: r.guzman@fz-juelich.de

Number of pages: 37

Number of figures: 12 main figures; 3 tables

24 **Number of words:** abstract (188/250), significant statement (117/120) introduction (523/650), and
25 discussion (1463/1500)

26 **Conflict of interest:**

27 The authors declare that the research was conducted in the absence of any commercial or financial
28 relationships that could be construed as a potential conflict of interest.

29 **Acknowledgments**

30 We are grateful to Petra Thelen for excellent technical assistance in molecular biology, to Verena Graf for
31 her assistance in the quantitative PCR experiments and to Dr. Nicola Kornadt-Beck and the staff of our
32 animal facility for invaluable support in all aspects of the animal work. This work was supported by a
33 grant from the Deutsche Forschungsgemeinschaft (DFG) (GU 2042/2-1) to REG.

34 **ABSTRACT**

35 CIC-3, CIC-4, and CIC-5 are electrogenic chloride/proton exchangers that can be found in endosomal
 36 compartments of mammalian cells. Although the association with genetic diseases and the severe
 37 phenotype of knockout animals illustrate their physiological importance, the cellular functions of these
 38 proteins have remained insufficiently understood. We here study the role of two *Clcn3* splice variants,
 39 CIC-3b and CIC-3c, in granular exocytosis and catecholamine accumulation of adrenal chromaffin cells
 40 using a combination of high-resolution capacitance measurements, amperometry, protein expression/gene
 41 knock-out/down, rescue experiments, and confocal microscopy. We demonstrate that CIC-3c resides in
 42 immature as well as in mature secretory granules, where it regulates catecholamine accumulation and
 43 contributes to the establishment of the readily releasable pool of secretory vesicles. The lysosomal splice
 44 variant CIC-3b contributes to vesicle priming only with low efficiency and leaves the vesicular
 45 catecholamine content unaltered. The related Cl^-/H^+ antiporter CIC-5 undergoes age-dependent down-
 46 regulation in wild-type conditions. Its upregulation in *Clcn3*^{-/-} cells partially rescues the exocytotic mutant
 47 defect. Our study demonstrates how different CLC transporters with similar transport functions, but
 48 distinct localizations can contribute to vesicle functions in the regulated secretory pathway of granule
 49 secretion in chromaffin cells.

50

51 **Significance Statement**

52 Cl^-/H^+ exchangers are expressed along the endosomal/lysosomal system of mammalian cells, however,
 53 their exact subcellular functions have remained insufficiently understood. We used chromaffin cells, a
 54 system extensively used to understand presynaptic mechanisms of synaptic transmission, to define the
 55 role of CLC exchangers in neurosecretion. Disruption of CIC-3 impairs catecholamine accumulation and
 56 secretory vesicle priming. There are multiple CIC-3 splice variants, and only expression of one, CIC-3c,
 57 in double Cl^-/H^+ exchanger-deficient cells fully rescues the WT phenotype. Another splice variant, CIC-
 58 3b, is present in lysosomes and is not necessary for catecholamine secretion. The distinct functions of

59 CIC-3c and CIC-3b illustrate the impact of expressing multiple CLC transporters with similar transport
 60 functions and separate localizations in different endosomal compartments.

61 INTRODUCTION

62 Adrenal chromaffin cells are prototypic neuroendocrine cells and represent a well-established model for
 63 studying presynaptic nerve terminals at high temporal resolution. They release catecholamine into
 64 systemic circulation by exocytosis of large dense-core vesicles (LDCVs), which accumulate
 65 catecholamines via proton-coupled vesicular monoamine transporters (Yaffe et al., 2018). In chromaffin
 66 cells, LDCVs are organized in four different vesicle pools, the depot pool (DP), the unprimed pool (UPP),
 67 the slowly releasable pool (SRP), and the readily releasable pool (RRP) (Becherer & Rettig, 2006).
 68 Vesicles move from the depot pool to the membrane and form the unprimed pool (UPP) in a process
 69 known as docking. Subsequently, in the Ca^{2+} -dependent step, the transition of vesicles from UPP to the
 70 slowly releasable pool (from which vesicles transit towards the RRP) is defined as priming (Becherer &
 71 Rettig, 2006). Physiological stimuli cause an elevation of intracellular calcium concentrations and mainly
 72 trigger fusion of release-competent or “primed” vesicles from the RRP (Voets *et al.*, 1999), making this
 73 vesicle pool the principal determinant of the high spatio-temporal accuracy of catecholamine secretion
 74 (Dhara et al., 2014, Mishima et al., 2014, Schoch et al., 2001, Sorensen et al., 2003).

75 CLC chloride transporters have been proposed to contribute to vesicular acidification,
 76 neurotransmitter filling, and trafficking of intracellular organelles in various cells (Stauber et al., 2010,
 77 Stauber et al., 2013). Adrenal chromaffin cells express all CLC antiporters (Maritzen et al., 2008), but
 78 their functions and subcellular localizations have remained largely controversial (Barg et al., 2001, Deriy
 79 et al., 2009, Jentsch et al., 2010, Li et al., 2009, Maritzen et al., 2008). In experiments using CIC-3
 80 antibodies with KO staining-controlled specificity, Maritzen et al. (2008) did not find CIC-3 in secretory
 81 granules of adrenal chromaffin cells and pancreatic islet cells. The authors observed reduced exocytotic
 82 responses and lower catecholamine content in *Clcn3*^{-/-} chromaffin cells and postulated an indirect role of
 83 this transporter in exocytosis. Other groups reported localization in secretory vesicles and direct
 84 regulation of intra-granular pH and secretion of insulin-containing granules by CIC-3 in pancreatic β -cells

85 (Barg et al., 2001, Deriy et al., 2009), however, antibodies were not tested for specificity in *Clcn3*^{-/-}
86 animals.

87 There are multiple splice variants of *Clcn3*, and, thus far, the contributions of these distinct CIC-3
88 splice variants to chromaffin function have not been addressed. We combined high-resolution membrane
89 capacitance measurements, amperometric recordings, and confocal images to identify cellular roles of
90 CIC-3 splice variants. We aimed to determine the subcellular localization of CIC-3b and CIC-3c and
91 elucidated at which vesicular maturation step Cl⁻/H⁺ exchanger regulates exocytosis in chromaffin
92 granules. We found that the exocytosis of secretory granules and their catecholamine content are reduced
93 in the absence of CIC-3. Rescue experiments from double Cl⁻/H⁺ exchanger-deficient cells revealed that
94 expression of CIC-3c fully restore transmitter content and granule exocytosis. Expression of CIC-3b did
95 not alter catecholamine accumulation of single secretory granules, but partially rescued exocytosis in cells
96 lacking CIC-3 and CIC-5. Our results demonstrate that CIC-3c is present in a subpopulation of large
97 dense-core vesicles and directly regulates catecholamine accumulation and exocytosis in chromaffin cells,
98 whereas CIC-3b contributes to the priming of secretory granules, but is not involved in the process of
99 neurotransmitter accumulation.

100 **Materials and Methods**

101 *Mutant mice and cell culture*

102 *Cln3*^{-/-} mice - kindly provided by Dr. Thomas Jentsch (Leibniz-Forschungsinstitut für Molekulare
103 Pharmakologie, Berlin, Germany) (Stobrawa et al., 2001) – were maintained as heterozygotes by
104 continuous crossbreeding with C57BL/6. Knockout and WT littermates of either sex were obtained by
105 crossing heterozygotes and were identified by PCR genotyping. Preparation and cultivation of adrenal
106 chromaffin cells were performed as described previously (Borisovska et al., 2005, Sorensen et al., 2003).
107 In brief, adrenal glands were removed and enzymatically treated (12 U/ml papain; Worthington
108 Biochemical Corporation) for 20 min. Subsequently, cells were seeded on glass coverslips after trituration
109 and cultured at 37°C and 10% CO₂ in enriched DMEM (100 ml DMEM supplemented with 0.4 ml
110 penicillin/streptomycin, 1 ml sodium pyruvate 100 mM and 1 ml insulin-transferrin-selenium-X; Gibco).
111 For lentiviral transduction, the viral suspension was added 2h after plating. Patch-clamp and
112 amperometric recordings were performed at room temperature either on the second or third day in vitro
113 (DIV), or 4-5 after infection of the cells with viral particles. For confocal microscopy, cells were seeded
114 on poly-D-lysine (Sigma-Aldrich, P6407) coated coverslips.

115

116 *Electrophysiology*

117 Whole-cell voltage clamp recordings were performed using an EPC10 amplifier controlled by
118 PatchMaster (HEKA Elektronik, GmbH). Photolysis of caged Ca²⁺ and ratiometric measurements of
119 intracellular calcium concentration were carried out as described (Borisovska et al., 2005). The standard
120 extracellular solution consisted of (in mM) 130 NaCl, 4 KCl, 2 CaCl₂, 1 MgCl₂, 10 HEPES, 48 D-
121 glucose, pH 7.4 with NaOH. For flash photolysis experiments pipettes with resistances between 3-4 MΩ
122 were filled with (in mM) 110 Cs-Glutamate, 8 NaCl, 3.5 CaCl₂, 5 NP-EGTA (kindly provided by Dr. D.
123 Bruns, University of Homburg, Germany), 0.2 Fura-2, 0.3 Furaptra (ThermoFisher), 2 MgATP, 0.3
124 Na₂GTP, 40 HEPES, (pH 7.3), 320 mOsm. NP-EGTA was photolyzed by a flash of ultraviolet light

125 (Xenon flash lamp, Rapp OptoElectronics, Hamburg, Germany) focused through an Olympus objective
 126 (60x, UPlanSApo, 1.35 oil) of an inverted microscope (IX71, Olympus, Hamburg, Germany). Fura-2 and
 127 Furaptra were excited at 350/380 nm using a monochromator light. To maintain high $[Ca^{2+}]_{int}$ after the
 128 flash small amounts of NP-EGTA were photolyzed. For quantifying depolarization-induced secretion we
 129 used patch pipettes with resistances between 3-4 M Ω and containing (in mM): 120 Cs-glutamate, 8 NaCl,
 130 0.18 CaCl₂, 0.28 BAPTA, 1 MgCl₂, 2 MgATP, 0.5 Na₂GTP, 10 HEPES-CsOH, pH 7.3, 350 nM
 131 calculated free $[Ca^{2+}]_{int}$, 290 mOsm, pH 7.4. Capacitances were measured using the Lindau-Neher
 132 technique (sine wave stimulus: 1000 Hz, 35 mV peak-to-peak amplitude, DC-holding potential -70 mV)
 133 using the lock-in extension of Patchmaster (HEKA, Elektronik, GmbH). Currents were low-pass filtered
 134 at 2.9 kHz and digitalized with a sampling rate of 20 kHz. Membrane capacitance was analyzed using
 135 SigmaPlot 12.3 software with customized routines (Systat Software). The flash-evoked capacitance
 136 response was fit with $f(t) = A_0 + A_1(1 - \exp^{-t/\tau_1}) + A_2(1 - \exp^{-t/\tau_2}) + kt$. A_0 denotes the cell capacitance before
 137 the flash, and A_1 , τ_1 and A_2 , τ_2 represent amplitudes and time constants of RRP and SRP, respectively
 138 (Rettig & Neher, 2002). Ca^{2+} currents from cultured chromaffin cells were measured as described by to
 139 Toft-Bertelsen *et al* (2016). The standard extracellular solution contained (in mM) 135 NaCl, 10 HEPES,
 140 2.8 KCl, 10 CaCl₂, 1 MgCl₂, 11 d-glucose, and 1 μ M tetrodotoxin. The patch-pipette solution contained
 141 (in mM) 112.5 CsGlut, 36 4-(2-hydroxyethyl)piperazine-1-ethanesulfonic acid (HEPES), 9 NaCl, 3
 142 MgATP, 0.45 Na₂GTP, and 10 EGTA (300 mOsm, pH 7.2). Ca^{2+} currents were measured during 100 ms
 143 test pulses ranging from -70 to +120 mV in 10 mV increments from a holding potential of -70 mV. We
 144 determined the voltage dependence of channel activation by plotting tail current amplitudes measured at
 145 fixed test step to -50 mV following the variable test pulses applied.

146 Carbon fiber electrodes (7 μ m diameter, GoodFellow, Cambridge, England) were prepared as
 147 previously described (Guzman et al., 2007). Amperometric recordings were performed under voltage
 148 clamp conditions with a polarization potential of +800 mV, filtered at 2.9 kHz and sampled at 20 kHz,
 149 and analyzed using Origin (OriginLab) and an Igor-based macro developed in Sulzer lab
 150 (sulzerlab.org/download.html) (IgorPro 7.01 Software, Wavemetrics). The analysis was restricted to

151 events with peak amplitude > 7 pA, total charge > 10 fC, and 50-90% rise time faster than 0.9ms. Foot
 152 signal events > 2 ms in duration were analyzed. For K^+ -induced secretion, the external solution (in mM:
 153 50 NaCl, 80 KCl, 2 $CaCl_2$, 1 MgCl, 48 glucose, 10 HEPES, pH 7.3 adjusted with NaOH) was applied
 154 from a perfusion pipette. Only one recording was made per coverslip to avoid the fatigue of the secretory
 155 response. For calcium infusion experiments the pipettes solution contained (in mM): 110 Cs-glutamate, 8
 156 NaCl, 1 $CaCl_2$, 20 DPTA, 1 MgCl₂, 2 MgATP, 0.5 Na₂GTP, 40 HEPES-CsOH, pH 7.3, 3 μ M calculated
 157 free $[Ca^{2+}]_{int}$.

158

159 *Expression constructs and lentiviral production*

160 We constructed the RNA-polymerase III promoter based on the lentiviral backbone vector FsY 1.1-eGFP
 161 G.W. (kindly provided by Dr. M. Filippov, Nizhny Novgorod, Russia). The human H1 promoter was
 162 cloned upstream of the synapsin promoter (H1-FsY1.1-eGFP), and the short-hairpin targeting sequence
 163 found in the mouse CIC-5 nucleotide sequence NM_016691.2 (CCTATGATGATTTCACACAA) was
 164 cloned downstream of the H1 promoter (H1-shRNA-FsY 1.1-eGFP), (Sigma, Clone ID: NM_016691.2-
 165 240s1c1, TCR number: TCRN0000069494, mean knockdown level of 94% and mean knockdown level
 166 tested in chromaffin cell cultures was of 92.6%, $n = 8$ cultures). In addition, a scrambled shRNA sequence
 167 (ACTACCGTTGTTATAGGTG) was inserted into the same vector and used as a control for all shRNA
 168 experiments (H1-shRNA_{scr}-FsY 1.1-eGFP). To rescue CIC-3 function, the CIC-3 promoter was cloned
 169 downstream of the H1-shRNA sequence replacing the synapsin promoter (H1-shRNA-FpromCIC-3 1.1-
 170 eGFP). We cloned the *Mus musculus* CIC-3b and CIC-3c sequence downstream to the CIC-3 promoter,
 171 followed by 2A self-cleaving sequence and eGFP. (FpromCIC-3c 1.1-eGFP or H1-shRNA- FpromCIC-3c
 172 1.1-eGFP). The genomic localization of the promoter sequence used in this study is chromosome 8,
 173 NC_000074.6 (from 60955251 to 60954643). This position is located right in front of the starting codon
 174 of CIC-3c and is different from the promoter sequence of the other CIC-3 splice variants. CIC-3c
 175 (Genebank Nr. NM_173876.3) or CIC-3b (Genebank Nr. NM_173873.1) (O'Leary et al, 2016). An empty
 176 vector carrying CIC-3c promoter and eGFP was used as a control (FpromCIC-3c 1.1-eGFP). Lentiviral

177 particles were produced as described (Guzman et al., 2010) by co-expressing lentiviral expression vectors,
 178 the helper plasmids pRSVREV, pMDLg/pRRE, and vesicular stomatitis virus G protein-expressing
 179 plasmid (kindly provided by Dr. Thomas Südhof (Howard Hughes Medical Institute, Stanford University)
 180 in HEK293FT cells. The culture medium containing lentiviral particles was collected 72 h post-
 181 transfection and ultracentrifuged for 2 h. Lentiviral particles were immediately resuspended in culture
 182 medium, frozen in liquid nitrogen, and stored at -80°C.

183

184 *Confocal microscopy*

185 Lentiviral transduction was used to express CIC-3b and CIC-3c (Guzman et al., 2015) in combination
 186 with fluorescent markers such as Lamp1 (which was a gift from Walther Mothes, Addgene plasmid #
 187 1817) (Sherer et al., 2003), Rab7, Rab11 (a gift from Richard Pagano, Addgene plasmid # 12605)
 188 (Choudhury et al., 2002), TfR (a gift from Gary Banker, Addgene plasmid # 45060) (Burack et al., 2000),
 189 VAMP3 and VAMP4 (were a gift from Thierry Galli, Addgene plasmid # 42310 and # 42313) (Galli et
 190 al., 1998), chromogranin A and neuropeptide Y were cloned into the p156rrL lentivector (Guzman et al.,
 191 2010) using genomic cDNA isolated from mouse adrenal gland and using the following set of primers;
 192 Chromogranin A (Genebank Nr. NM_007693.2) (O'Leary et al., 2016) forward 5'-
 193 ATGCGCTCCACCGCGGTTCTG-3', reverse 5'-TCCCCGCCGCAAAGCCTGC-3' and neuropeptide Y
 194 (Genebank Nr. NM_023456.3) (O'Leary et al., 2016), forward 5'-
 195 ATGCTAGGTAACAAGCGAATGGGGC-3' and reverse 5'-CCACATGGAAGGGTCTTCAAGCC-3'.
 196 Chromaffin cells were imaged 4-5 days after transduction with a Leica TCS SP5 II inverted microscope
 197 (Leica Microsystems, Wetzlar, Germany) using a 63x oil immersion objective in PBS containing Ca^{2+} and
 198 Mg^{2+} (GIBCO) at room temperature (22-24°C). eGFP (enhance green fluorescence proteins) fluorophore
 199 was excited with a 488-nm Argon laser, mRFP (monomeric red fluorescence protein) with a 594-nm He-
 200 Ne laser, and emission signals were detected after filtering at 500-550 nm or 600-650 nm bandpass filters.
 201 WT or *Cln3*^{-/-} chromaffin cells from P0-P1 were used for immunostaining after four days of culture.
 202 Cells were fixed for 10 min with 4% paraformaldehyde and permeabilized for 1h with a solution

203 containing; 0.5 % triton 100, 5% fetal bovine serum, and 0.5% bovine serum albumin in phosphate buffer,
 204 pH 7.4. Thereafter the samples were immunostained using the primary CIC-3 antibodies, rabbit anti-CIC-
 205 3 ACL-001 from Alomone labs or rabbit anti-CIC-3 C9602 from sigma-Aldrich at the concentration
 206 suggested by the manufactures or using 1:100 dilution (both concentrations gave similar results), and
 207 mouse anti-chromogranin A (Ab8204, Abcam) or with mouse anti-LAMP1 (H4A3 Sc-20011, Santa Cruz)
 208 using the concentrations recommended by the manufacture. Samples were washed twice and incubated
 209 with the secondary antibody (rabbit Alexa 488 and mouse Alexa 647, 1:1000 in phosphate buffer, A-
 210 11008, and A-31571 from Invitrogen). To determine the degree of co-localization between CIC-3b or
 211 CIC-3c or the anti-CIC-3 ACL-001 antibody and the different intracellular markers, the subcellular
 212 localization was quantified in confocal images as mRFP fluorescence intensity overlapping with eGFP
 213 fluorescence or Alexa 488 fluorescence intensity overlapping with Alexa 647 signal using Mander's
 214 overlap coefficient. Images were analyzed and assembled for publications in ImageJ 1.44p software
 215 (National Institutes of Health, Bethesda, USA) (Schneider et al., 2012).

216

217 *Electron microscopy*

218 Adrenal glands from WT and *Clcn3*^{-/-} littermates (P0-P1) were fixed for 24 hours with 2.5%
 219 glutaraldehyde in 0.1 M phosphate buffer at room temperature. After fixation, glands were washed with
 220 phosphate buffer for further 24 hours, treated with 1% OsO₄ (in 0.2 M phosphate buffer) for 3 hours,
 221 washed twice with distilled water, and dehydrated using ascending alcohol concentrations (25 to 100%).
 222 Dehydrated glands were incubated with propylene oxide followed by additional 20 min incubation with a
 223 1:1 mixture of epon: propylene oxide (epon; 47.5% glycidether, 26.5% dodenylsuccinic acid anhydride,
 224 24.5% methylnadic anhydride, and 1.5% Tris (dimethylaminomethyl)phenol). Thereafter, samples were
 225 immersed in pure epoxy resin for 1 hour at room temperature followed by polymerization (28 °C for 8
 226 hours, 80 °C for 2.5 hours, and finally at RT for 4 hours). Ultra-thin sections (approx. 60 to 80 nm
 227 thickness) were mounted on copper grids. To enhance contrast, sections were treated with uranyl acetate
 228 and lead citrate. Samples were examined using an EM900 electron microscope (Zeiss, Germany)

229 equipped with a slow-scan CCD-Camera (TRS, Germany). We only used sections containing cells with
 230 visible nucleus and identified secretory vesicles by their round electron-dense core. For each condition,
 231 different fields of view were analyzed, the number of vesicles was counted in this area and the diameter
 232 of secretory vesicles was measured. Data are presented as mean \pm s.e.m with *n* indicating the number of
 233 vesicle. Statistical comparisons were made using One-Way ANOVA (Turkey test).

234

235 *RNA isolation and qRT-PCR*

236 Adrenal glands were collected from C57BL/6 mouse strain at two different developmental stages, P0
 237 (n=5 mice) and P60 (n=3) or *Clcn3*^{-/-} mice at P0 (n=5). RNA was isolated using the TRIzol Reagent
 238 method following the manufacturer's instruction (Thermo Fisher Scientific, Ref. 15596026). In brief,
 239 20 mg of tissue sample were homogenized in 1 ml of TRIzol, mixed with chloroform, and vigorously
 240 shaken for 15 s. After 2-3 min incubation at room temperature, the sample was centrifugated at 12.000 g
 241 for 20 min at 4°C. The upper aqueous phase containing the RNA was separated, mixed with isopropanol
 242 by vortexing, and incubated for 10 min at room temperature. After centrifugation at 12.000 g for 10 min
 243 at 4°C, the supernatant was discarded and the pellet was washed with 75% ethanol, vortexed, and
 244 centrifuged at 7.500 g for 5 min at 4°C. The pellet was dried for 15-20 min and resuspended in 20 μ l of
 245 RNAase-free water. Genomic DNA was eliminated by treating the isolated RNA with DNAase using the
 246 DNAase I kit (Thermo Fisher Scientific, Ref. 18068015). To evaluate the expression of the different CIC
 247 exchangers we performed RT-PCR using 1 μ g of total RNA, SuperScript III One-step RT-PCR system
 248 (Invitrogen, Ref. 12574) and the following set of primers; CIC-3a (Genebank Nr. NM_007711.3)
 249 (O'Leary et al., 2016); 5'-CGCCCAGCTTGCTATGCCTCTGAG-3', reverse 5'-
 250 AGCTAGTGCCCCTGATGCCAGTC-3'; CIC-3b (Genebank Nr. NM_173873.1) (O'Leary et al., 2016)
 251 5'-CGCCCAGCTTGCTATGCCTCTGAG-3', reverse 5'-AGCTAGTGCCCCTGATGCCAGTC-3';
 252 CIC-3c (Genebank Nr. NM_173876.3) (O'Leary et al., 2016) 5'-ATGGATGCTTCTTCTGATCC-3',
 253 reverse 5'-AGCTAGTGCCCCTGATGCCAGTC-3'; CIC-3e (Genebank Nr. NM_173874.1) (O'Leary et
 254 al., 2016) 5'-TGCCCTCAGAAGAGACCTGACTATTGC-3', reverse 5'-

255 AACGAACTTCCTCTTCTGTCTCCTCTCTG-3'; CIC-5 isoform 2 (Genebank Nr. NM_001243762.1)
 256 (O'Leary et al., 2016) 5'-CAGAGGCTTTCATCAGGGGAGTTTTAG-3', reverse 5'-
 257 CTCAGAATTCCAGCAACAGTGCTCATG-3'; and the reference gene 18S rRNA 5'-
 258 CGCCGCTAGAGGTGAAATTCTTG-3', reverse 5'-GTGGCTGAACGCCACTTGTCC-3' was used.
 259 For quantitative RT-PCR (qRT-PCR), cDNA from the total RNA was synthesized by mixing 1 µg of total
 260 RNA with 2.5 µM oligo(dT)18 (Thermo Fisher Scientific Ref. SO132) and heating the mixture for 5 min
 261 at 65°C. After brief centrifugation, RNaseOUT recombinant RNase inhibitor (Thermo Fisher Scientific,
 262 Ref. 10777-019, 40 units/µl) and SuperScript III RT (200 units/µl) were added. The samples were
 263 incubated at 50°C for 1 h, subsequently inactivated at 70°C for 15 min and the newly synthesized cDNA
 264 was used for qRT-PCR. Control reactions using no reverse transcriptase or substituting cDNA with water
 265 were run in parallel for each sample. Two sets of gene-specific primers were designed for CIC-3 and CIC-
 266 5 to recognize sequences in the coding region of the mouse *Cln3* (Genebank Nr. NM_007711.3) and
 267 *Cln5* (Genebank Nr. NM_001243762.1) that allow amplification of the all existing splice variants; for
 268 CIC-3, forward 5'-CCTCTTATGGCTGCAGTAATGACC-3', reverse 5'-
 269 GCACTGCCTCAGACCAAGCTT-3'; CIC-5, forward 5'-CAGAGGCTTTCATCAGGGGAGTTTTAG-
 270 3' reverse 5'-CTCAGAATTCCAGCAACAGTGCTCATG-3' and for the reference genes 18S (Genebank
 271 Nr. NR_003278.3), forward 5'-CGCCGCTAGAGGTGAAATTCTTG-3', reverse 5'-
 272 GTGGCTGAACGCCACTTGTCC-3' and GFP forward 5'-TTCATCTGCACCACCGGCAA-3', reverse
 273 5'-TTGGGGTCTTTGCTCAGGGC-3'. The qRT-PCR was performed on 96 well plates using the
 274 Maxima SYBER Green qPCR Master Mix (Thermo Fisher Scientific, Ref. K0251) and run on a BIORAD
 275 instrument (thermal cycle C1000 Touch, CFX96 real-time system). The transcription levels of CIC-3 and
 276 CIC-5 were analyzed and compared to that of the reference gene (18S). Three separate analyses of PCR
 277 were performed. The data were analyzed according to the CFX manager (Bio-Rad) recommended
 278 protocols.

279

280 *Statistical analysis*

281 Statistical calculations were performed using SigmaPlot software (Version 12.3), Systat Software, San
 282 Jose, CA and Origin(Pro) (Version 2018), OriginLab Corporation, Northampton, MA, USA. All
 283 summary data are given as mean \pm s.e.m (standard error of the mean). The comparison was made using a
 284 *t*-test of means or ANOVA after passing assumptions of normality (Shapiro-Wilk test) and equal
 285 variances (Levene's test) or Mann-Whitney Rank Sum test with * $p < 0.05$, ** $p < 0.01$, *** $p < 0.001$ levels
 286 of significance. Grubbs test was performed to test for outliers.

287
 288 **Animal's maintenance**

289 The animals were maintained according to the guidelines of the federation of European laboratory Animal
 290 Science Association (FELASA) and the breeding for the CIC-3^{KOT^{je}} mouse line was approved by the
 291 Landesamt für Natur, Umwelt und Verbraucherschutz Nordrhein-Westfalen (LANUV), Aktenzeichen No
 292 84-02.04.2015.A108.

293
 294 **Author Contributions**

295 MC, designed and performed the confocal experiments and qPCR, analyzed the data; JS, performed the
 296 depolarization and high K⁺-induced secretion and amperometric experiments and analyzed the data; GGC
 297 and PH, performed the calcium current experiments and analyzed the data; AF, performed the molecular
 298 biology experiments; IK, performed the electron microscopy experiments; AW, performed the qPCR
 299 experiments and analyzed the data; ChF, supervised the research and wrote the manuscript; REG,
 300 performed the depolarization and high K⁺-induced secretion, flash photolysis, amperometric, confocal,
 301 qPCR and molecular biology experiments, analyzed the data, designed the experimental strategy, and
 302 wrote the manuscript.

303 RESULTS

304 CIC-3 regulates granule exocytosis in chromaffin cells

305 We studied granule exocytosis in chromaffin cells from newborn and adult mice upon trains of
 306 depolarizing pulses using time-resolved capacitance measurements. Such pulses increase $[Ca^{2+}]_i$ at the
 307 plasma membrane via activation of voltage-gated calcium channels and trigger the fusion of vesicles that
 308 are in close proximity to the calcium channels. We employed a series of depolarizations (18 pulses,
 309 100 ms to +10 mV delivered with 300 ms resting intervals at -70mV) that is known to effectively deplete
 310 the RRP within the first four pulses of the stimulus trains, but to be ineffective in releasing vesicles from
 311 the SRP (Voets *et al.*, 1999). In chromaffin cells prepared from newborn mice, the total capacitance
 312 changes elicited by this stimulation protocol were larger in *Clcn3*^{-/-} chromaffin cells than in WT.
 313 However, the fourth step of depolarization, which defines the size of the RRP, was not different between
 314 WT and *Clcn3*^{-/-} (Fig. 1A-C). The amplitude of the Ca^{2+} current component during the first four
 315 depolarization episodes was on average 1.4 ± 0.08 fold higher in chromaffin cells isolated from young
 316 *Clcn3*^{-/-} mice than for WT (Fig. 1D). Na^+ currents were not altered in young *Clcn3*^{-/-} cells (Fig. 1E). In
 317 cells from adult mice, we found the first four capacitance responses within the stimulus train to be
 318 reduced in *Clcn3*^{-/-} (Fig. 1F-H), with unchanged calcium and sodium current amplitudes (Fig. 1I-J).
 319 Since exocytosis is triggered by Ca^{2+} influx in these experiments, the age-dependent differences might be
 320 due to regulatory adjustments in the number or function of voltage-gated Ca^{2+} channels. We therefore
 321 isolated Ca^{2+} currents with Cs^+ -based intracellular solution and 2 μ M of tetrodotoxin in the bath solution
 322 to block K^+ and Na^+ currents, these experiments revealed a 1.5 ± 0.25 fold increase in peak calcium
 323 current amplitudes in juvenile *Clcn3*^{-/-} cells, with no changes in the voltage dependence of channel
 324 activation (Fig. 2A-D). Adult *Clcn3*^{-/-} cells did not show differences in the peak calcium current
 325 amplitudes when compared to the WT.

326 Constitutive genetic ablation often causes compensatory changes in expression levels of other
 327 proteins. Therefore, we hypothesized that other proteins with similar functions as CIC-3, for example,
 328 CIC-4 or CIC-5, might compensate exocytosis in the *Clcn3*^{-/-} condition at an early developmental stage

and increase the number of voltage-gated calcium channels at the plasma membrane. CIC-4 and CIC-5 are also present in adrenal glands (Maritzen *et al.*, 2008) and exhibit comparable functional properties as CIC-3 (Guzman *et al.*, 2013). Since CIC-4 lacks an endosomal trafficking signal and requires association with CIC-3 to be exported from the endoplasmic reticulum (ER) to endosomal compartments (Guzman *et al.*, 2017), it is unlikely that CIC-4 exerts direct effects on exocytosis in *Clcn3*^{-/-} condition. Therefore, we focused on CIC-5 and quantified mRNA transcripts levels in WT mice at two different ages, P0 and P60. We found CIC-5 transcripts to be reduced by about 70% in adult mouse adrenal tissue as compared to WT newborn condition (Log [cDNA] = 2.7±0.2 for CIC-5 in WT P0 vs for CIC-5 in WT P60 = 1.8±0.2, *p* = 0.02, Table 1). Moreover, CIC-5 expression is upregulated in *Clcn3*^{-/-} adrenal glands, (Log [cDNA] = 2.7±0.2 for CIC-5 in WT P0 vs in 3.1±0.15 for CIC-5 in *Clcn3*^{-/-} P0, *p* = 0.02, Table 1). Altogether, these data show an age-dependent reduction in the CIC-5 mRNA expression levels that are associated with changes in the density of voltage-gated calcium channels.

CIC-3c localizes to a subpopulation of LDCVs that is positive for VAMP3/cellubrevin

There are five splice variants of *Clcn3*, CIC-3a, CIC-3b, CIC-3c, CIC-3d, and CIC-3e, which reside in distinct intracellular compartments (Gentzsch *et al.*, 2003, Guzman *et al.*, 2015, Okada *et al.*, 2014). We tested the expression of CIC-3 in mouse adrenal glands using RT-PCR and found not only all *Clcn3* splice variants, but also CIC-5 in this tissue (Fig. 3A). In cultured mammalian cells, CIC-3a and CIC-3b localize to the lysosome (Guzman *et al.*, 2015) and CIC-3e to the Golgi apparatus (Gentzsch *et al.*, 2003). The exact subcellular localization of CIC-3d is currently not known; however, carboxy-terminal sequences are identical in CIC-3d and CIC-3e suggesting that CIC-3d also localizes to Golgi (Okada *et al.*, 2014) (Fig. 4A). CIC-3c is sorted to the recycling endosome of HEK293T cells (Guzman *et al.*, 2015) and thus represents a candidate Cl⁻/H⁺ exchanger in chromaffin cell LDCVs.

Since there are no CIC-3-specific antibodies available that permit distinction between endosomal CIC-3 splice variants (Fig. 5), we expressed CIC-3b and CIC-3c as eGFP-fusion proteins in chromaffin cells and studied their subcellular localization using confocal microscopy and Mander's correlation

coefficient (Fig. 4B-E). To avoid overexpression artifact, we used the mouse CIC-3c promoter to drive the expression of CIC-3. Cells transduced with the exogenous CIC-3b or CIC-3c reached nearly the same mRNA transcripts levels as in the WT condition (endogenous CIC-3c $6.3\text{e-}3 \pm 0.4\text{e-}3$ vs exogenous CIC-3c $7.0\text{e-}3 \pm 0.3\text{e-}3$ $p=0.1$ and endogenous CIC-3b $2.1\text{e-}2 \pm 0.4\text{e-}2$ vs exogenous CIC-3b $2.2\text{e-}2 \pm 1.0\text{e-}2$ $p=0.1$; $n = 4-5$ cultures, Mann-Whitney Rank Sum test). Chromaffin cells were co-transfected with fluorescently tagged markers, such as VAMP3/cellubrevin, VAMP4, Chromogranin A (ChrA), or neuropeptide Y (NPY), were co-expressed together with CIC-3c or CIC-3b. VAMP3 is a vSNARE protein present in recycling endosomes (Teter et al., 1998) and implicated in the exocytosis of chromaffin granules (Borisovska et al., 2005); NPY and ChrA are markers for LDCVs (Huttner et al., 1995), and VAMP4 has been used to identify immature LDCVs (Bonnemaïson et al., 2013, Eaton et al., 2000). We found CIC-3c, but not CIC-3b, preferentially in a subpopulation of LDCV that are positive for VAMP3 (Fig. 4B(a), 4E(a), and 4D). CIC-3b localizes to lysosomes (Fig. 4E(c) and 4D), in agreement with Maritzen et al. (2008), but not to the recycling endosome (Fig. 4E(b) and 4D). In contrast, more than 70% of CIC-3c positive puncta co-localize with VAMP3 and more than 50% with NPY or ChrA and with VAMP4 (Fig. 4B(b-d) and 4D). There are two functionally distinct populations of recycling endosomes that either express Rab11 (Kobayashi & Fukuda et al., 2013) or the transferrin receptor TfR (Maxfield et al., 2004). In agreement with our previous work (Guzman et al. 2015), we found co-localization of CIC-3c with both recycling endosomal marker Rab11 and TfR (Kobayashi & Fukuda, 2013, Ullrich et al., 1996) (Fig. 4C(a-b), 4D), whereas co-localization with the lysosomal/late endosomal marker Lamp1/Rab7 was negligible (Fig. 4E(d), 4D and Fig. 6). These results identify CIC-3c as the CIC-3 splice variant present at a subpopulation of VAMP3-positive LDCVs.

Expression of CIC-3c but not of CIC-3b fully rescues exocytosis in double mutant *Clcn3^{-/-}/kdCIC-5* cells

Photolytic uncaging of Ca^{2+} causes a homogeneous step-like increase in the intracellular calcium concentration ($[\text{Ca}^{2+}]_i$) from ~ 300 nM to ~ 30 μM that synchronizes fusion of catecholamine-containing

381 vesicles and permits quantifying the time course of vesicle fusion (Fig. 7A). In such experiments, three
 382 kinetically distinct release components can be separated by fitting the capacitance time course with the
 383 sum of two exponentials and a linear function: the exocytotic burst (EB), in which the rapidly releasable
 384 (RRP) and the slowly releasable pool of vesicles (SRP) fuse with the membrane (Voets et al., 1999), and
 385 the sustained component, which reflects the continuous priming and fusion of granules at high $[Ca^{2+}]_i$
 386 (Rettig et al., 2002). When calcium channels are bypassed with flash photolysis, the absence of CIC-3
 387 indeed attenuates the exocytotic response in young cells (Fig. 7). The exocytotic burst as well as its two
 388 components of release, the RRP and SRP are reduced in *Clcn3*^{-/-}+*Scr* cells (Fig. 7B-7D), without changes
 389 in time constants, and the sustained component of release remains unaltered. The reduced changes in
 390 membrane cell capacitance during exocytotic bursts might be due to smaller vesicles in the *Clcn3*^{-/-}
 391 condition. We quantified LDCV's size by electron microscopy (EM) and did not find differences in
 392 LDCV's size distributions between *Clcn3*^{-/-} and WT condition from P0-P1 mice (Fig. 8A and 8B). On
 393 average, we obtained LDCVs diameters of 141.3±2.6 nm in WT and 147.7±5.0 nm in *Clcn3*^{-/-} ($p=0.3$,
 394 Mann-Whitney Rank Sum test, Fig. 8C), similar to values reported for mice at this age (Pineiro et al.,
 395 2014). We conclude that the absence of CIC-3 does not alter the size of the LDCVs in chromaffin cells,
 396 but rather the availability of vesicles for exocytosis.

397 We next corrected for the upregulation of CIC-5 in *Clcn3*^{-/-} by using lentivirus-mediated short
 398 hairpin RNA transfer (shRNA) (*Clcn3*^{-/-}/*kdCIC-5* in the following denoted as double mutant (*DMut*)
 399 cells). As controls WT or *Clcn3*^{-/-} cells were transduced with a virus carrying the scrambled shRNA
 400 sequence (denoted as + *Scr*). *DMut* cells showed a significant reduction of the CIC-5 mRNA expression
 401 levels 4-5 days after lentiviral transduction (mRNA CIC-5 levels relative to 18S for WT+*Scr* = 0.014 ±
 402 1.5e-3 and for *kdCIC-5* = 9.62e-4±1.99e-5, $p<0.003$, $n = 8$ cultures, student's *t*-test). Deletion of CIC-5 in
 403 *Clcn3*^{-/-} cells leads to a further reduction of the exocytotic burst in the flash-evoked vesicle exocytosis by
 404 around 40% (*Clcn3*^{-/-}+*Scr* 264.2±20.8 fF vs *DMut* 158.9±15.3 fF, $p<0.001$) so that responses of *DMut*
 405 chromaffin cells were 54% smaller than in WT+*Scr* cells (WT+*Scr* 349.1±11.9 fF vs *DMut*
 406 158.9±15.3 fF, $p<0.001$) (Fig. 7A and 7B). Reduced CIC-5 expression in *Clcn3*^{-/-} cells mainly impaired

the size of the fast phase (RRP), whereas the slow phase (SRP) of the exocytotic burst remained almost unaffected (Fig. 7C and 7D). The subsequent sustained component of the release, as well as the release time constant of the RRP, were not altered by the absence of both transporters (*DMut*). Knockdown of CIC-5 in WT cells did not change the exocytotic response (Fig. 7, orange trace and circles), arguing against an independent upstream function of CIC-5 in granule exocytosis.

Expression of CIC-3c in *Dmut* cells completely restores the flash-evoked response (Fig. 7B-7D). The exocytotic burst and its two components of release were significantly different from the *DMut*, but similar to control (Fig. 7B-7D). CIC-3b expression was less effective in rescuing the exocytotic response (Fig. 7A). The magnitude of the exocytotic burst was similar in *Dmut*+CIC-3b cells to that observed in *Clcn3*^{-/-}+*Scr* cells (Fig. 7B). The size of the RRP was almost identical to the *Clcn3*^{-/-}+*Scr* condition, but significantly higher than that of the *Dmut* cells, and the SRP was not statistically different from the *Dmut* (Fig. 7C and 7D). Expression of the exogenous CIC-3c or 3b in *Dmut* cells resulted in similar mRNA transcript levels of the splice variants as in the WT condition (endogenous CIC-3c 6.3e-3±0.4e-3 vs exogenous CIC-3c 7.0e-3±0.3e-3 *p*=0.1 and endogenous CIC-3b 2.1e-2±0.4e-2 vs exogenous CIC-3b 2.2e-2±1.0e-2 *p*=0.1; *n* = 4-5 cultures, Mann-Whitney Rank Sum test). We can therefore exclude the possibility that the rescue phenotypes are a consequence of lentiviral CIC-3c or CIC-3b overexpression. The rescue experiments indicate that CIC-3c is sufficient to support granule exocytosis and can fully substitute for the loss of Cl⁻/H⁺ exchangers in secretory vesicles. They suggest that CIC-3c is present in LDCVs, in good agreement with our confocal results.

CIC-3c but not CIC-3b contributes to catecholamine accumulation in secretory granules

The absence of CIC-3 Cl⁻/H⁺ exchangers is predicted to alter the luminal ionic composition of chromaffin granules and thus their neurotransmitter content. To assess the catecholamine content of individual secretory vesicles and define the contribution of CIC-3c and CIC-3b to catecholamine accumulation, we used carbon fiber amperometry and stimulated secretion by extracellular application of 80 mM of potassium solution or by infusion of 3μM of free Ca²⁺. Upon stimulation with high K⁺ - that mimic

433 electrical stimulation with >15Hz (Fulop and Smith, 2007) - spike amplitudes and charges (which reports
 434 on the vesicular catecholamine content) as well as frequencies of the amperometric signal were
 435 significantly smaller in *DMut* than in WT+*Scr* (Fig. 9A-E); half-width and 50-90% rise times were
 436 unchanged (Fig. 9F and 9G). No differences in any amperometric parameter were observed between
 437 *Clcn3^{-/-}*+*Scr* and *Dmut* (Fig. 9B-9G). Expression of CIC-3c in *DMut* cells restored WT event frequency,
 438 amplitude, and charge (Fig. 9B-9D). In contrast, expression of CIC-3b in *DMut* left quantal sizes as small
 439 as in *DMut* cells (Fig. 9B-9D), with no changes in the half-width and in the rise time (Fig. 9F and 9G).
 440 Event frequency in *Dmut*+CIC-3b cells was not significantly different from the *Dmut* or WT+*Scr*,
 441 however, frequencies values were below those obtained in WT+*Scr* or *Dmut*+CIC-3c conditions (Fig.
 442 9E). The foot signal (Table 2) was comparable for WT and in absence of both transporters and not
 443 changed upon expression of CIC-3b or CIC-3c, indicating that Cl⁻/H⁺ exchangers are not involved in the
 444 fusion pore formation of secretory granules.

445 Infusion of 3 μM free Ca²⁺ permits resolving individual secretory responses independently of
 446 voltage-gated calcium channel opening. However, Ca²⁺ infusion does not only trigger the fusion of highly
 447 primed vesicles, but also the unprimed pool of vesicles. In *Dmut*, amperometry experiments confirmed
 448 the reduced catecholamine content of secretory granules in the absence of both transporters (Fig. 10,
 449 *Dmut*). The amplitude, frequency, and quantal charge were significantly reduced in *Dmut* cells when
 450 compared to the WT+*Scr* condition (Fig. 10A-10E). The half-width of *Dmut* fusion events triggered by
 451 intracellular Ca²⁺ infusion was larger than WT+*Scr*-mediated events (Fig. 10B and 10F), but unaltered
 452 upon stimulation by K⁺ perfusion. Expression of CIC-3c rescued the frequency and the quantal size in
 453 *DMut* cells also for this stimulation paradigm to WT levels (Fig. 10C-10E). The rescue was only evident
 454 during the first 40 s of amperometric recording, suggesting that only newly formed vesicles were
 455 equipped with the transduced protein (Duncan et al., 2003, Estevez-Herrera et al., 2016) (Fig. 11). Again,
 456 expression of CIC-3b in *Dmut* cells (*Dmut*+CIC-3b) failed to restore the catecholamine content of the
 457 individual secretory granules; quantal amplitude and charge were significantly smaller than the WT+*Scr*,
 458 but not statistically different from *Dmut* (Fig 10C and 10E). Event frequency was not different between

459 *Dmut*+CIC-3b and *Dmut*. CIC-3b and CIC-3c did not cause major changes in foot signal or in the 50-90%
 460 rise time of the amperometry currents (Table 3 and Fig 10G), reinforcing the notion that Cl^-/H^+
 461 exchangers are not involved in the formation and expansion of the fusion pore of secretory granules.
 462 Expression of CIC-3b or CIC-3c both accelerated the half-width to values closer to WT+*Scr* condition
 463 (Fig 10F). The presence of CIC-3c but not of CIC-3b in secretory vesicles is in line with the notion that
 464 Cl^-/H^+ exchangers are required to regulate the vesicular catecholamine content of chromaffin granules.

465

466 DISCUSSION

467 We here studied the role of CLC Cl^-/H^+ exchangers in chromaffin cells. We found that one CIC-3 splice
 468 variant, CIC-3c, localizes to the LDCVs, regulates the catecholamine accumulation process, and
 469 efficiently contributes to the establishment of secretory granules for exocytosis. CIC-3b is not present in
 470 LDCVs, and does not regulate the granular neurotransmitter content. It contributes to vesicle priming, but
 471 only with reduced efficiency. CIC-5 is developmentally down-regulated in WT chromaffin cells, and CIC-
 472 3 deficiency causes compensatory changes in the CIC-5 mRNA expression levels.

473 The contribution of Cl^-/H^+ exchangers to granule exocytosis in chromaffin cells can be
 474 demonstrated in rescue experiments, in which exocytosis was triggered by flash photolysis of caged
 475 calcium (Fig. 7). The expression of CIC-3c in double Cl^-/H^+ exchanger-deficient cells fully rescues the
 476 exocytotic response of secretory granules to WT levels (Fig. 7, *Dmut*+CIC-3c), showing that CIC-3c is
 477 essential and functionally sufficient for neurosecretion. In contrast, the expression of CIC-3b in *Dmut*
 478 cells supports exocytosis with low-efficiency (Fig. 7, *Dmut*+CIC-3b). In the absence of CIC-3,
 479 upregulation of CIC-5 (Table 1) was not able to compensate for the flash-evoked response (Fig. 7, *Clcn3*^{-/-}
 480 +*Scr*). Its removal in WT cells does not alter granule exocytosis (Fig. 7, WT+*kdCIC-5*), indicating that
 481 CIC-5 plays a minor, if any, role in exocytosis in WT condition.

482 To study the fusion of individual vesicles we employed two different experimental approaches,
 483 high K^+ or Ca^{2+} -infusion stimulation (Fig. 9, and Fig. 10). We used amperometry to analyse the quantal
 484 neurotransmitter content of the chromaffin granules and found reduced quantal amperometric charges in

the absence of CIC-3 alone (*Clcn3*^{-/-}, Fig. 9) or absence of CIC-3 and CIC-5 (*DMut*) (Fig. 9 and Fig. 10). Since the size of LDCVs is similar in WT and *Clcn3*^{-/-} (Fig. 8), such reduction must be caused by differences in LDCV catecholamine concentrations. In rescue experiments from *Dmut* cells, the expression of CIC-3c was the only Cl⁻/H⁺ exchanger that fully recovers all amperometric parameters to control levels (Fig. 9 and Fig. 10). Lentiviral expression of CIC-3b left quantal sizes in *DMut* cells unaffected (Fig. 9 and Fig. 10), indicating that only CIC-3c, but not CIC-3b contributes to catecholamine accumulation. None of our genetic maneuvers changed the pre-spike signal or the rise time of amperometric events (Table 2, Table 3, Fig. 9G, and Fig. 10G), arguing against an important role of CIC-3 in the initial formation and expansion of the fusion pores in chromaffin granules. Application of 80 mM of extracellular K⁺ as well as Ca²⁺-infusion lead to a fast increase in the cytosolic Ca²⁺ at the release site and promotes full-collapse vesicle exocytosis (Elhamdani et al. 2001 and Fulop and Smith, 2007). The observed smaller unitary events in *Dmut* under such full-collapse fusion exclude the possibility of partial catecholamine discharge from mutant granules.

This functional evidence is in good agreement with our co-localization analyses. It supports the notion that CIC-3c, but not CIC-3b, is present in LDCVs, with CIC-3c in a subpopulation of LDCV positive for VAMP3 and CIC-3b in lysosomes (Fig. 4). Our conclusion that CIC-3c is present in LDCVs disagrees with earlier reports on the CIC-3 localization in chromaffin cells. Maritzen and colleagues (2008) used immuno-labeling and viral infection to conclude that CIC-3 neither co-localizes with chromogranin in chromaffin cells, a marker for secretory granules, nor with insulin in β -pancreatic cells. The discrepancy between these and our results is likely due to the existence of multiple splice variants with distinct subcellular localization. The antibodies used in the earlier study cannot differentiate between splice variants, and Maritzen et al. (2008) virally expressed only CIC-3b, so that no conclusion can be drawn about CIC-3c from these experiments. Recently, Weinert et al. (2020) used localization experiments with fluorescently tagged CIC-3 and functional studies to conclude that CIC-3 is not present in synaptic vesicles. They took advantage of a novel knock-in mouse model (*Clcn3*^{ven/ven}) with a Venus tag sequence fused to the start of exon 1. This genetic modification results in the expression of only

511 certain fluorescently tagged *Clcn3* splice variants, i.e. of CIC-3a (M_007711.3), but not of others, most
 512 importantly not of CIC-3c. Moreover, Weinert and colleagues (2020) assessed synaptic transmission in
 513 hippocampal slices and found that the frequency and amplitude of quantal events were similar between
 514 WT and *Clcn3*^{-/-}, however, the authors did not correct for the upregulation of CIC-5 at the age, in which
 515 the experiments were performed (P14-16). The novel experiments of Weinert et al. (2020) thus do not
 516 contradict the functional role of CIC-3c in exocytosis.

517 CLC antiporters might affect the recycling of other proteins that regulate catecholamine secretion.
 518 Genetic ablation of SNAP-25, a SNARE protein essential for Ca²⁺-dependent exocytosis in
 519 neuroendocrine cells, causes defective priming of LDCVs (Sørensen et al., 2003, Washbourne et al.,
 520 2002) and alters Ca²⁺ current densities in chromaffin cells (Toft-Bertelsen et al., 2016), quite similar to
 521 the *Clcn3*^{-/-} phenotype. However, deletion of SNAP-25 leaves the neurotransmitter content of individual
 522 granules unaffected (Sørensen et al., 2003) thus excluding the possibility that a trafficking defect of
 523 SNAP-25 is the sole basis of the observed functional alterations. Secretory vesicles contain a granule
 524 matrix that binds catecholamines (Helle et al., 1985). Two major constituents, chromogranin A and B,
 525 have been identified and shown to be involved in granulogenesis as well as in catecholamine
 526 sequestration (Diaz-Vera et al., 2012, Kim et al., 2006, Videen et al., 1992, Yoo, 1996). The absence of
 527 chromogranin A/B in chromaffin cells reduces the quantal charge and the frequency of amperometric
 528 events (Diaz-Vera et al., 2012), similar to the *DMut* phenotype. However, whereas deletion of
 529 chromogranin A/B affects the rising phase of quantal events, the *DMut*-mediated events do not show
 530 changes in the kinetic of fusion, neither by high K⁺ stimulation nor by Ca²⁺-infusion the rise-time was
 531 affected by the double CLC deletion (Fig. 9 and Fig. 10). This indicates that a reduced granular content of
 532 granins is not responsible for the *DMut* phenotype.

533 Fig. 12 depicts our current concepts about the functions of CIC-3b and CIC-3c in chromaffin
 534 cells. After exocytosis, chromaffin granule components are retrieved through the early endosome to the
 535 trans-Golgi network (Ceridono et al., 2011), and nascent granules undergo additional maturation steps
 536 that involve reduction of the luminal pH (Kim et al., 2006). VMATs exchange one catecholamine for two

537 luminal protons, so that pH gradients across the LDCV membrane are main determinants of the vesicular
 538 catecholamine content. CIC-3 is a chloride/proton exchanger, and its pronounced voltage dependence
 539 makes CIC-3 perfectly suited for chloride-driven vesicle acidification (Guzman et al., 2013, Rohrbough et
 540 al., 2018). Our results are compatible with the idea that CIC-3c regulates the catecholamine accumulation
 541 process by fine-tuning the luminal ion concentration of secretory vesicles. CIC-3c traffics from the trans-
 542 Golgi network to recycling endosomes (RE) and consequently to immature secretory granule, where it
 543 might contribute to reducing the luminal pH as maturation step. Lack of CIC-3 impairs vesicle
 544 acidification and makes catecholamine accumulation less efficient, resulting in lower levels of
 545 neurotransmitters. CIC-3b contributes to vesicle priming (Fig. 7C, *Dmut*+CIC-3b) and is unable to restore
 546 the quantal content (Fig. 9 and Fig. 10, *Dmut*+CIC-3b), suggesting that CIC-3b is present at an early stage
 547 of vesicle maturation and is subsequently sorted to the lysosomes (Fig. 12). In addition to modifying the
 548 vesicular ion homeostasis, CIC-3 might also recruit novel binding partners that modify secretory vesicle
 549 pools (Weinert et al., 2014).

550 We observed increased densities of voltage-gated calcium channels (Fig. 2) and CIC-5 mRNA
 551 transcript levels in chromaffin cells from young *Clcn3*^{-/-} mice (Table 1). Moreover, exocytosis elicited by
 552 a train of depolarizing pulses was significantly impaired in adults, but not in young *Clcn3*^{-/-} cells (Fig. 1).
 553 These results suggest that CIC-5 regulates the trafficking of calcium channels in an early developmental
 554 stage. *CLCN5* is the disease gene for Dent's disease (Fisher et al., 1995), and its gene product, CIC-5, was
 555 shown to be involved in endocytosis of various epithelial cells (Piwon et al., 2000). Age-dependent
 556 downregulation in neuronal tissues, as well as the lack of neurological symptoms in Dent's disease
 557 patients (Wrong et al., 1994), suggested that CIC-5 does not play an important role in the mature central
 558 nervous system. Our work on chromaffin cells - a model system for presynaptic function - demonstrates
 559 how regulating the expression of CIC-5 minimizes the impact of CIC-3 ablation on exocytosis by
 560 increasing the number of calcium channels on the plasma membrane. This mechanism predicts a
 561 neuroprotective function of CIC-5 in neuronal cells, which likely prevents neurodegeneration in *Clcn3*^{-/-}
 562 before P20 (Stobrawa et al., 2001).

Our results identify CIC-3 as key elements of the regulated exocytotic pathway of neuroendocrine cells. They indicate that CIC-3c plays an active role in the neurotransmitter accumulation process, most likely adjusting luminal ionic concentrations of secretory vesicles and thereby facilitating catecholamine uptake. This work pinpoints the subcellular role of CIC-3 in neuroexocytosis and sets down the bases for a better understanding of the functions of Cl⁻/H⁺ exchangers in cellular physiology.

REFERENCES

- Barg S, Huang P, Eliasson L, Nelson DJ, Obermüller S, Rorsman P, Thevenod F, Renström E (2001) Priming of insulin granules for exocytosis by granular Cl⁻ uptake and acidification. *J Cell Sci* 114: 2145-2154
- Becherer U, Rettig J (2006) Vesicle pools, docking, priming, and release. *Cell Tissue Res* 326: 393-407
- Bonnemaison ML, Eipper BA, Mains RE (2013) Role of adaptor proteins in secretory granule biogenesis and maturation. *Front Endocrinol* 4: 101
- Borisovska M, Zhao Y, Tsytysyura Y, Glyvuk N, Takamori S, Matti U, Rettig J, Sudhof T, Bruns D (2005) v-SNAREs control exocytosis of vesicles from priming to fusion. *EMBO J* 24: 2114-2126
- Burack MA, Silverman MA, Banker G (2000) The role of selective transport in neuronal protein sorting. *Neuron* 26: 465-472
- Ceridono M, Ory S, Momboisse F, Chasserot-Golaz S, Houy S, Calco V, Haeberle AM, Demais V, Bailly Y, Bader MF, Gasman S (2011) Selective recapture of secretory granule components after full collapse exocytosis in neuroendocrine chromaffin cells. *Traffic* 12: 72-88
- Choudhury A, Dominguez M, Puri V, Sharma DK, Narita K, Wheatley CL, Marks DL, Pagano RE (2002) Rab proteins mediate Golgi transport of caveola-internalized glycosphingolipids and correct lipid trafficking in Niemann-Pick C cells. *J Clin Invest* 109: 1541-1550

586 Deriy LV, Gomez EA, Jacobson DA, Wang X, Hopson JA, Liu XY, Zhang G, Bindokas VP, Philipson
 587 LH, Nelson DJ (2009) The granular chloride channel CIC-3 is permissive for insulin secretion. *Cell*
 588 *Metab* 10: 316-323

589 Dhara M, Yarzagaray A, Schwarz Y, Dutta S, Grabner C, Moghadam PK, Bost A, Schirra C, Rettig J,
 590 Reim K, Brose N, Mohrmann R, Bruns D (2014) Complexin synchronizes primed vesicle exocytosis and
 591 regulates fusion pore dynamics. *J Cell Biol* 204: 1123-1140

592 Diaz-Vera J, Camacho M, Machado JD, Dominguez N, Montesinos MS, Hernandez-Fernaund JR, Lujan
 593 R, Borges R (2012) Chromogranins A and B are key proteins in amine accumulation, but the
 594 catecholamine secretory pathway is conserved without them. *FASEB J* 26: 430-438

595 Duncan RR, Greaves J, Wiegand UK, Matskevich I, Bodammer G, Apps DK, Shipston MJ, Chow RH
 596 (2003) Functional and spatial segregation of secretory vesicle pools according to vesicle age. *Nature* 422:
 597 176-80

598 Eaton BA, Haugwitz M, Lau D, Moore HP (2000) Biogenesis of regulated exocytotic carriers in
 599 neuroendocrine cells. *J Neurosci* 20: 7334-7344

600 Elhamdani A, Palfrey HC, Artalejo CR (2001) Quantal size is dependent on stimulation frequency and
 601 calcium entry in calf chromaffin cells. *Neuron* 31: 819-30

602 Estevez-Herrera J, Dominguez N, Pardo MR, Gonzalez-Santana A, Westhead EW, Borges R, Machado
 603 JD (2016) ATP: The crucial component of secretory vesicles. *Proc Natl Acad Sci U S A* 113: E4098-106

604 Fisher SE, van Bakel I, Lloyd SE, Pearce SH, Thakker RV, Craig IW (1995) Cloning and characterization
 605 of CLCN5, the human kidney chloride channel gene implicated in Dent disease (an X-linked hereditary
 606 nephrolithiasis). *Genomics* 29: 598-606

- 607 Fulop T, Smith C (2007) Matching native electrical stimulation by graded chemical stimulation in
 608 isolated mouse adrenal chromaffin cells. *J Neurosci Methods* 166: 195-202
- 609 Galli T, Zahraoui A, Vaidyanathan VV, Raposo G, Tian JM, Karin M, Niemann H, Louvard D (1998) A
 610 novel tetanus neurotoxin-insensitive vesicle-associated membrane protein in SNARE complexes of the
 611 apical plasma membrane of epithelial cells. *Mol Biol Cell* 9: 1437-1448
- 612 Gentzsch M, Cui L, Mengos A, Chang XB, Chen JH, Riordan JR (2003) The PDZ-binding chloride
 613 channel CIC-3B localizes to the Golgi and associates with cystic fibrosis transmembrane conductance
 614 regulator-interacting PDZ proteins. *J Biol Chem* 278: 6440-6449
- 615 Guzman RE, Bolanos P, Delgado A, Rojas H, DiPolo R, Caputo C, Jaffe EH (2007) Depolymerisation
 616 and rearrangement of actin filaments during exocytosis in rat peritoneal mast cells: involvement of
 617 ryanodine-sensitive calcium stores. *Pflugers Arch* 454: 131-141
- 618 Guzman RE, Bungert-Plumke S, Franzen A, Fahlke C (2017) Preferential association with CIC-3 permits
 619 sorting of CIC-4 into endosomal compartments. *J Biol Chem* 292: 19055-19065
- 620 Guzman RE, Grieschat M, Fahlke C, Alekov AK (2013) CIC-3 is an intracellular chloride/proton
 621 exchanger with large voltage-dependent nonlinear capacitance. *Acs Chem Neurosci* 4: 994-1003
- 622 Guzman RE, Miranda-Laferte E, Franzen A, Fahlke C (2015) Neuronal CIC-3 splice variants differ in
 623 subcellular localizations, but mediate identical transport functions. *J Biol Chem* 290: 25851-25862
- 624 Guzman RE, Schwarz YN, Rettig J, Bruns D (2010) SNARE force synchronizes synaptic vesicle fusion
 625 and controls the kinetics of quantal synaptic transmission. *J Neurosci* 30: 10272-10281
- 626 Helle KB, Reed RK, Pihl KE, Serck-Hanssen G (1985) Osmotic properties of the chromogranins and
 627 relation to osmotic pressure in catecholamine storage granules. *Acta Physiol Scand* 123: 21-33

- 628 Huttner WB, Ohashi M, Kehlenbach RH, Barr FA, Bauerfeind R, Braunling O, Corbeil D, Hannah M,
 629 Pasolli HA, Schmidt A *et al* (1995) Biogenesis of neurosecretory vesicles. *Cold Spring Harb Symp Quant*
 630 *Biol* 60: 315-327
- 631 Jentsch TJ, Maritzen T, Keating DJ, Zdebik AA, Thevenod F (2010) CIC-3--a granular anion transporter
 632 involved in insulin secretion? *Cell metabolism* 12: 307-308; author reply 309-10
- 633 Kim T, Gondre-Lewis MC, Arnaoutova I, Loh YP (2006) Dense-core secretory granule biogenesis.
 634 *Physiology* 21: 124-133
- 635 Kobayashi H, Fukuda M (2013) Arf6, Rab11 and transferrin receptor define distinct populations of
 636 recycling endosomes. *Commun Integr Biol* 6: e25036
- 637 Li DQ, Jing X, Salehi A, Collins SC, Hoppa MB, Rosengren AH, Zhang E, Lundquist I, Olofsson CS,
 638 Morgelin M, Eliasson L, Rorsman P, Renstrom E (2009) Suppression of sulfonylurea- and glucose-
 639 induced insulin secretion in vitro and in vivo in mice lacking the chloride transport protein CIC-3. *Cell*
 640 *Metab* 10: 309-315
- 641 Maritzen T, Keating DJ, Neagoe I, Zdebik AA, Jentsch TJ (2008) Role of the vesicular chloride
 642 transporter CIC-3 in neuroendocrine tissue. *J Neurosci* 28: 10587-10598
- 643 Maxfield FR, McGraw TE (2004) Endocytic recycling. *Nat Rev Mol Cell Biol* 5: 121-132
- 644 Mishima T, Fujiwara T, Sanada M, Kofuji T, Kanai-Azuma M, Akagawa K (2014) Syntaxin 1B, but not
 645 syntaxin 1A, is necessary for the regulation of synaptic vesicle exocytosis and of the readily releasable
 646 pool at central synapses. *PLoS One* 9: e90004
- 647 Okada T, Akita T, Sato-Numata K, Islam MR, Okada Y (2014) A newly cloned CIC-3 isoform, CIC-3d,
 648 as well as CIC-3a mediates Cd-sensitive outwardly rectifying anion currents. *Cell Physiol Biochem* 33:
 649 539-556

650 O'Leary NA, Wright MW, Brister JR, Ciufo S, Haddad D, McVeigh R, Rajput B, Robbertse B, Smith-
 651 White B, Ako-Adjei D *et al* (2016) Reference sequence (RefSeq) database at NCBI: current status,
 652 taxonomic expansion, and functional annotation. *Nucleic Acids Res* 44: D733-745.
 653 Piwon N, Gunther W, Schwake M, Bosl MR, Jentsch TJ (2000) CIC-5 Cl⁻-channel disruption impairs
 654 endocytosis in a mouse model for Dent's disease. *Nature* 408: 369-73
 655 Rettig J, Neher E (2002) Emerging roles of presynaptic proteins in Ca⁺⁺-triggered exocytosis. *Science*
 656 298: 781-78
 657 Rohrbough J, Nguyen HN, Lamb FS (2018) Modulation of CIC-3 gating and proton/anion exchange by
 658 internal and external protons and the anion selectivity filter. *J Physiol* 596: 4091-4119
 659 Schneider CA, Rasband WS, Eliceiri KW (2012) NIH Image to ImageJ: 25 years of image analysis. *Nat*
 660 *Meth* 9: 671-675
 661 Schoch S, Deak F, Konigstorfer A, Mozhayeva M, Sara Y, Sudhof TC, Kavalali ET (2001) SNARE
 662 function analyzed in synaptobrevin/VAMP knockout mice. *Science* 294: 1117-1122
 663 Sherer NM, Lehmann MJ, Jimenez-Soto LF, Ingmundson A, Horner SM, Cicchetti G, Allen PG, Pypaert
 664 M, Cunningham JM, Mothes W (2003) Visualization of retroviral replication in living cells reveals
 665 budding into multivesicular bodies. *Traffic* 4: 785-801
 666 Sorensen JB, Nagy G, Varoqueaux F, Nehring RB, Brose N, Wilson MC, Neher E (2003) Differential
 667 control of the releasable vesicle pools by SNAP-25 splice variants and SNAP-23. *Cell* 114: 75-86
 668 Stauber T, Jentsch TJ (2010) Sorting motifs of the endosomal/lysosomal CLC chloride transporters. *J*
 669 *Biol Chem* 285: 34537-34548
 670 Stauber T, Jentsch TJ (2013) Chloride in vesicular trafficking and function. *Annu Rev Physiol* 75: 453-
 671 477

- 672 Stobrawa SM, Breiderhoff T, Takamori S, Engel D, Schweizer M, Zdebik AA, Bosl MR, Ruether K, Jahn
673 H, Draguhn A, Jahn R, Jentsch TJ (2001) Disruption of CLC-3, a chloride channel expressed on synaptic
674 vesicles, leads to a loss of the hippocampus. *Neuron* 29: 185-196
- 675 Teter K, Chandy G, Quinones B, Pereyra K, Machen T, Moore HP (1998) Cellubrevin-targeted
676 fluorescence uncovers heterogeneity in the recycling endosomes. *J Biol Chem* 273: 19625-19633
- 677 Toft-Bertelsen TL, Ziolkiewicz I, Houy S, Pinheiro PS, Sorensen JB (2016) Regulation of Ca²⁺ channels
678 by SNAP-25 via recruitment of syntaxin-1 from plasma membrane clusters. *Mol Biol Cell* 27: 3329-3341
- 679 Ullrich O, Reinsch S, Urbe S, Zerial M, Parton RG (1996) Rab11 regulates recycling through the
680 pericentriolar recycling endosome. *J Cell Biol* 135: 913-924
- 681 Videen JS, Mezger MS, Chang YM, O'Connor DT (1992) Calcium and catecholamine interactions with
682 adrenal chromogranins. Comparison of driving forces in binding and aggregation. *J Biol Chem* 267:
683 3066-3073
- 684 Voets T, Neher E, Moser T (1999) Mechanisms underlying phasic and sustained secretion in chromaffin
685 cells from mouse adrenal slices. *Neuron* 23: 607-615
- 686 Washbourne P, Thompson PM, Carta M, Costa ET, Mathews JR, Lopez-Bendito G, Molnar Z, Becher
687 MW, Valenzuela CF, Partridge LD, Wilson MC (2002) Genetic ablation of the t-SNARE SNAP-25
688 distinguishes mechanisms of neuroexocytosis. *Nat Neurosci* 5: 19-26
- 689 Weinert S, Gimber N, Deuschel D, Stuhlmann T, Puchkov D, Farsi Z, Ludwig CF, Novarino G, Lopez-
690 Cayuqueo KI, Planells-Cases R, Jentsch TJ (2020) Uncoupling endosomal CLC chloride/proton exchange
691 causes severe neurodegeneration. *EMBO J* 39: e103358
- 692 Weinert S, Jabs S, Hohensee S, Chan WL, Kornak U, Jentsch TJ (2014) Transport activity and presence
693 of CLC-7/Ostm1 complex account for different cellular functions. *EMBO Rep* 15: 784-791

- 694 Wrong OM, Norden AG, Feest TG (1994) Dent's disease; a familial proximal renal tubular syndrome
695 with low-molecular-weight proteinuria, hypercalciuria, nephrocalcinosis, metabolic bone disease,
696 progressive renal failure and a marked male predominance. *QJM* 87: 473-493
- 697 Yaffe D, Forrest LR, Schuldiner S (2018) The ins and outs of vesicular monoamine transporters. *J Gen*
698 *Physiol* 150: 671-682
- 699 Yoo SH (1996) pH- and Ca^{2+} -dependent aggregation property of secretory vesicle matrix proteins and the
700 potential role of chromogranins A and B in secretory vesicle biogenesis. *J Biol Chem* 271: 1558-1565.

701 **FIGURE LEGENDS**

702 **Figure 1. Exocytosis triggered by trains of depolarizing steps is impaired in *Clcn3*^{-/-} cells from adult**
 703 **mice**

704 **A**, Schematic representation of the depolarization protocol used to trigger exocytosis of secretory vesicles
 705 (upper panels; 18 pulses, 100 ms to +10 mV delivered with 300 ms rest intervals) and the lower panel
 706 shows the averaged ΔCm responses from WT and for *Clcn3*^{-/-} cells obtained from P0 mice. **B**, Mean value
 707 for the total ΔCm in newborn WT or *Clcn3*^{-/-} chromaffin cells. **C**, Mean sizes of the RRP from newborn
 708 WT or *Clcn3*^{-/-} chromaffin cells. **D, E**, The amplitude of the Ca^{2+} currents measured during the first 4
 709 depolarization episodes but not of the Na^{+} currents measured at the first depolarization step, was
 710 significantly higher in the *Clcn3*^{-/-} chromaffin cells from young mice. **F**, Schematic representation of the
 711 depolarization protocol used to trigger secretion (upper panel, 18 pulses, 100 ms to +10 mV delivered
 712 with 300 ms rest intervals) and the lower panel shows the averaged ΔCm responses in adult WT or *Clcn3*^{-/-}
 713 cells. **G**, Mean value for the total ΔCm from adult WT or *Clcn3*^{-/-} cells. **H**, Mean sizes of the RRP
 714 from adult WT or *Clcn3*^{-/-} cells. **I, J**, The amplitude of the Ca^{2+} currents measured during the first 4
 715 depolarization episodes and Na^{+} currents measured at the first depolarization step were similar between
 716 WT and *Clcn3*^{-/-} chromaffin cells isolated for adult mice. Young mice: WT, $n=25$, black circles; *Clcn3*^{-/-}
 717 $n=26$, red circles and adult mice: WT, $n=29$, black circles; *Clcn3*^{-/-} $n=35$, red circles, *** $p<0.001$,
 718 ** $p<0.01$, * $p<0.05$, *ns* (not significant). Student's *t*-test. Data were collected from five independent
 719 experiments per condition and are represented as mean \pm s.e.m.

720 **Figure 2. Calcium currents are increased in *Clcn3*^{-/-} cells from young mice**

721 **A**, Voltage protocol to activate VGCC (upper panel) and representative calcium currents of WT (in black)
 722 and *Clcn3*^{-/-} (in red) cells from young animals. **B**, Deletion of CIC-3 increases calcium current amplitudes
 723 when compared with WT chromaffin cells, (WT, $n=25$, black circles, and *Clcn3*^{-/-}, $n=29$, red circles). **C**,
 724 Voltage dependence of steady-state current amplitudes for WT (in black) or *Clcn3*^{-/-} (in red) chromaffin

725 cells. **D**, Deletion of CIC-3 does not affect the voltage dependence of calcium current activation, WT
 726 ($n=17$, in black) and *Clcn3*^{-/-} ($n=20$, in red). **E**, Voltage protocol to activate VGCC (upper panel) and
 727 representative calcium currents of WT (in black) and *Clcn3*^{-/-} (in red) cells from adult animals. **F**, In
 728 contrast to young, *Clcn3*^{-/-} adult chromaffin cells do not show changes in the peak of calcium current
 729 amplitude when compared to the control, (WT, $n=20$, black circles, and *Clcn3*^{-/-}, $n=21$, red circles). **G**,
 730 Voltage dependence of steady-state current amplitudes for WT (in black) or *Clcn3*^{-/-} (in red) chromaffin
 731 cells from adult mice. Note that the peak of the calcium current amplitude measured in chromaffin cells
 732 from adult mice has shifted 10 mv to the right (+20 mv) when compared to those measured from young
 733 cells. **H**, Deletion of CIC-3 does not affect the voltage dependence of calcium current activation, WT
 734 ($n=20$, in black) and *Clcn3*^{-/-} ($n=21$, in red). ** $p<0.01$, *ns* (not significant). Student's *t*-test. Data were
 735 collected from four independent experiments per condition and are represented as mean \pm s.e.m. *n*, which
 736 denotes the number of analyzed cells.

737 **Figure 3. Expression of CIC-3 and CIC-5 in mouse adrenal gland**

738 **A**, The expression of Cl⁻/H⁺ exchangers in adrenal glands was examined by RT-PCR. The expected PCR
 739 product size obtained for each transporter revealed the presence of mRNA transcripts of CIC-3 splice
 740 variants and CIC-5 in this tissue. Mouse adrenal glands were collected from five P0-1 old mice and
 741 pooled together.

742 **Figure 4. Subcellular localization of CIC-3 splice variants**

743 **A**, Diagram of the protein topology model of CIC-3 illustrating the transmembrane and cytoplasmic
 744 domains. The 18 α helices are labeled from A-R, the two cytoplasmic cystathionine beta-synthase (CBS)
 745 domains are shown in ovals (CBS1 and CBS2). The amino acid sequence of the cytoplasmic N- and C-
 746 amino terminus are shown within the rectangles. Highlighted in red, we illustrated the clathrin binding
 747 dileucine motif and in blue, the recycling endosomes targeting signal. Note that CIC-3b and CIC-3c differ
 748 only in the length and amino acid composition of the N-terminus. **B**, Confocal images of chromaffin cells
 749 expressing CIC-3c-eGFP/mRFP (CIC-3c promoter-driven expression) together with markers for large

750 dense-core vesicles. CIC-3c-eGFP/mRFP with; mRFP-VAMP3 (*a*), NPY-mRFP (*b*), Chromogranin
 751 ChrA-eGFP (*c*), mRFP-VAMP4 (*d*). **C**, Confocal pictures showing the co-localization of CIC-3c-eGFP in
 752 recycling endosomes, positive for mRFP-Rab11 (*a*) and transferrin receptor TfR-mRFP (*b*). **D**, Mander's
 753 coefficient analyses for all co-localization experiments. More than 70% of CIC-3c positive puncta co-
 754 localize with VAMP3, Rab11, or with TfR and more than 50 % with NPY, ChrA, or with VAMP4 but not
 755 with Lamp1 indicating that a large fraction of CIC-3c protein resides mainly in a subpopulation of LDCV
 756 positive for recycling endosomes (VAMP3). In contrast, CIC-3b shows extensive co-localization with
 757 LAMP1 but negligible co-localization with VAMP3 or with Rab11. Data were collected from 4
 758 independent cultures, CIC-3c/VAMP3, *n*=11; CIC-3c/NPY, *n*=12; CIC-3c/ChrA, *n*=11; CIC-3c/VAMP4,
 759 *n*=10; CIC-3c/Rab11, *n*=10; CIC-3c/TfR, *n*=10; CIC-3c/Lamp1, *n*=10; CIC-3b/VAMP3, *n*=16; CIC-
 760 3/Rab11, *n*=10; CIC-3b/Lamp1, *n*=12. All data are represented as mean \pm s.e.m. **E**, Representative
 761 confocal images from chromaffin cells co-expressing the splice variant CIC-3b-eGFP together with
 762 mRFP-VAMP3 (*a*) or with the recycling endosomal markers mRFP-Rab11 (*b*) or the lysosomal marker
 763 Lamp1-mRFP (*c*). Note that CIC-3b accumulates in the membrane of large vesicle structures that exhibit
 764 a high degree of co-localization with the lysosomal marker Lamp1 (*c*) but not with VAMP3 (*a*) nor with
 765 the recycling endosomal marker Rab11 (*b*). CIC-3c-eGFP describes different subcellular distribution than
 766 Lamp1-mRFP (*d*). Inset shows areas outlined in the white boxes. Line scan analyses (bottom panel of
 767 each confocal image) for the corresponding protein illustrating that subcellular distribution pattern at both
 768 channels (dashed lines). Scale bars 5 μ m and within the insets 1 μ m. *n* denotes the numbers of cells
 769 analyzed.

770
 771 **Figure 5. Commercially available CIC-3 antibodies are unspecific and failed in identifying CIC-3 in**
 772 **chromaffin cells.**

773 **A**, Confocal images of WT chromaffin cells from P0-P1 mice immunostained with CIC-3 antibody (ACL-
 774 001) together with chromogranin A (*a*), a marker for large dense-core vesicles or with LAMP1 (*b*), a
 775 lysosomal marker. **B**, Mander's coefficient analyses indicate not co-localization with chromogranin A

776 ($n=6$) or with LAMP1 ($n=6$). **C**, Confocal pictures of *Clcn3*^{-/-} chromaffin cells from P0-P1 mice
 777 immunostained with CIC-3 antibody (ACL-001) (*a*) or with CIC-3 antibody (C9602). Note that both
 778 antibodies stained intracellular structures in the absence of CIC-3. All data are represented as mean \pm
 779 s.e.m. Scale bars 5 μ m and within the insets 1 μ m. *n* denotes the numbers of cells analyzed. The
 780 immunostainings were performed from two different animals' preparations.

781 **Figure 6. CIC-3c does not localize to late endosomes**

782 **A**, Representative confocal image of chromaffin cells co-expressing CIC-3c-eGFP together with the late
 783 endosomal marker mRFP-Rab7. Inset shows areas outlined in the white boxes, dashed line within the
 784 image represents a linear section of the image analyzed in (**B**). Scale bars 5 μ m and within the inset 1 μ m.
 785 **B**, Line scan analysis, dashed line in (**A**), illustrating that CIC-3c exhibits a different subcellular
 786 distribution than Rab7. **C**, Mander's coefficient analysis for CIC-3c/Rab7 co-localization experiments.
 787 CIC-3c positive puncta do not co-localize with Rab7. CIC-3c/Rab7, $n=13$. Data are collected from three
 788 independent transfected cultures and represented as mean \pm s.e.m. *n*, which denotes the number of
 789 analyzed cells.

790 **Figure 7. Cl/H⁺ exchangers regulate exocytosis of LDCVs in chromaffin cells**

791 **A**, Averaged $[Ca^{2+}]_i$ (upper panel) and corresponding capacitance responses to flash stimulation from WT
 792 chromaffin cells expressing scrambled shRNA (WT+*Scr*, black trace) or shRNA against *Clcn5*
 793 (knockdown, WT+*kdCIC-5*, orange trace) or from *Clcn3*^{-/-} cells expressing scrambled shRNA (*Clcn3*^{-/-}
 794 +*Scr*, red trace) or shRNA against *Clcn5* (*DMut*; *Clcn3*^{-/-}+*kdCIC-5*, blue trace) or the different rescue
 795 conditions; CIC-3b or CIC-3c (*DMut*+CIC-3b, brown trace, and *DMut*+CIC-3c, gray trace). **B**, Changes of
 796 the exocytotic burst in response to flash stimulation from virally transduced WT or *Clcn3*^{-/-} chromaffin
 797 cells expressing different constructs (WT+*Scr*, $n = 14$, black circles, WT+*kdCIC-5*, $n = 14$, orange circles;
 798 *Clcn3*^{-/-}+*Scr*, $n = 23$, red circles; *DMut*, $n = 16$, blue circles; *DMut*+CIC-3b, $n = 19$, brown circles;
 799 *DMut*+CIC-3c, $n = 10$, gray circles). **C**, **D**, Knockdown of CIC-5 in *Clcn3*^{-/-} cells (*DMut*, blue circles)
 800 selectively reduce the size of the fast component of vesicle exocytosis (RRP) (**C**), leaving the slow

801 component (SRP) almost unaffected (**D**). Rescue experiments illustrate the ability of Cl^-/H^+ exchangers
 802 in restoring exocytosis of LDCVs in *Dmut* conditions. WT+*Scr*, $n = 14$, black circles; WT+*kdCIC-5*, $n =$
 803 14, orange circles; *Clcn3*^{-/-}+*Scr*, $n = 23$, red circles; *DMut*, $n = 16$, blue circles; *DMut*+CIC-3b, $n = 19$;
 804 *DMut*+CIC-3c, $n = 10$, gray circles. *** $p < 0.001$, ** $p < 0.01$ and *ns* (not significant). Groups of data were
 805 statistically analyzed by comparing them to WT+*Scr* or *Dmut* using one-way analysis of variance
 806 (Tukey's HSD post Hoc test). Data were collected from 4-5 independent cultures per condition and are
 807 represented as mean \pm s.e.m.

808 **Figure 8. Ablation of CIC-3 does not alter the size of LDCVs in chromaffin cells.**

809 **A**, Electron micrographs of a representative field of view from WT and *Clcn3*^{-/-} condition. **B**, histogram of
 810 the diameter distribution of LDCVs in electron micrograph from WT and *Clcn3*^{-/-} (black, WT, 580
 811 vesicles; red, *Clcn3*^{-/-}, 618 vesicles. **C**, Mean LDCV diameter (black, WT, 16 different fields of view; red,
 812 *Clcn3*^{-/-}, 14 different fields of view, $p = 0.3$), data were collected from two independent animal preparations
 813 and are represented as mean \pm s.e.m. *ns* (not significant). Student's *t*-test. Scale bar 1 μm .

814 **Figure 9. CIC-3c but not CIC-3b regulates catecholamine accumulation in chromaffin granules**

815 **A**, Representative amperometric traces for WT+*Scr*, *DMut*, or *DMut*+CIC-3c condition. Secretion of
 816 catecholamine was triggered by the application of a high K^+ -extracellular solution (80 mM KCl, 60 s
 817 duration). **B**, Representative single exocytotic events from amperometric recordings on WT+*Scr* (black),
 818 *Clcn3*^{-/-}+*Scr*, (red), *DMut* (blue), *DMut*+CIC-3b (brown), or *DMut*+CIC-3c (gray). **C-G**, Properties of
 819 secretory amperometric events for WT+*Scr* ($n = 24$, black circles), *Clcn3*^{-/-}+*Scr*, ($n = 20$, red circles),
 820 *DMut* ($n = 23$, blue circles), *DMut*+CIC-3b ($n = 21$, brown circles), or *DMut*+CIC-3c ($n = 25$, gray
 821 circles), represented as data distribution. *** $p < 0.001$, ** $p < 0.01$, * $p < 0.05$, *ns* (not significant), the
 822 different conditions were compared to WT+*Scr* or *DMut* using one-way analysis of variance (Tukey's
 823 HSD post Hoc test). Data were collected from 7 independent experiments per condition and are
 824 represented as mean \pm s.e.m.

825 **Figure 10. Ca^{2+} infusion experiments confirm the Cl^-/H^+ exchanger-dependency of the**
 826 **catecholamine accumulation process.**

827 **A**, Representative amperometric recording for WT, *DMut*, or *DMut*+CIC-3c (area highlighted in gray
 828 within the recording represents the first 40 s of analyses showed in C-G) stimulated by the pipette
 829 infusion of 3 μM free Ca^{2+} . **B**, Representative single exocytotic events from amperometric recordings on
 830 WT+Scr (black), *DMut* (blue), *DMut*+CIC-3b (brown), or *DMut*+CIC-3c (gray). Spikes with values closer
 831 to the mean average amplitude, charge, and half for each condition were selected within the amperometric
 832 recordings. **C-G**, Properties of secretory amperometric events for WT+Scr ($n = 23$ cells, black circles,
 833 with 63.5 ± 9.6 events per cells), *DMut* ($n = 20$ cells, blue circles; with 33.9 ± 4.5 events per cell),
 834 *DMut*+CIC-3b ($n = 18$ cells, brown circles; with 31.2 ± 5.46 events per cells), or *DMut*+CIC-3c ($n = 17$
 835 cells, gray circles; with 76.4 ± 7.7 events per cells), represented as data distribution. $***p < 0.001$,
 836 $**p < 0.01$, $*p < 0.05$, *ns* (not significant). Different conditions were compared to the WT+Scr or *Dmut*
 837 using one-way analysis of variance (Tukey's HSD post Hoc test). Data were collected from four
 838 independent experiments per condition and are represented as mean \pm s.e.m.

839 **Figure 11. Analyses of single amperometric events**

840 **A-B**, Properties of secretory amperometric events for WT+Scr ($n = 23$, black circles), *DMut* ($n=20$, blue
 841 circles), *DMut*+CIC-3b ($n=18$, brown circles), or *DMut*+CIC-3c ($n=17$, gray circles), represented data
 842 distribution within 40-80 s in (**A**) and 80-120 s and in (**B**) of amperometric recording. Data information:
 843 $***p < 0.001$, $**p < 0.01$, $*p < 0.05$, *ns* (not significant), Data were compared to WT+Scr using one-way
 844 analysis of variance (Tukey's HSD post Hoc test). Data were collected from 4-5 independent experiments
 845 per condition and are represented as mean \pm s.e.m. n , which denotes the number of analyzed cells.

846 **Figure 12. Proposed functions and subcellular localization of CLC-type Cl^-/H^+ exchangers in**
 847 **neurosecretion**

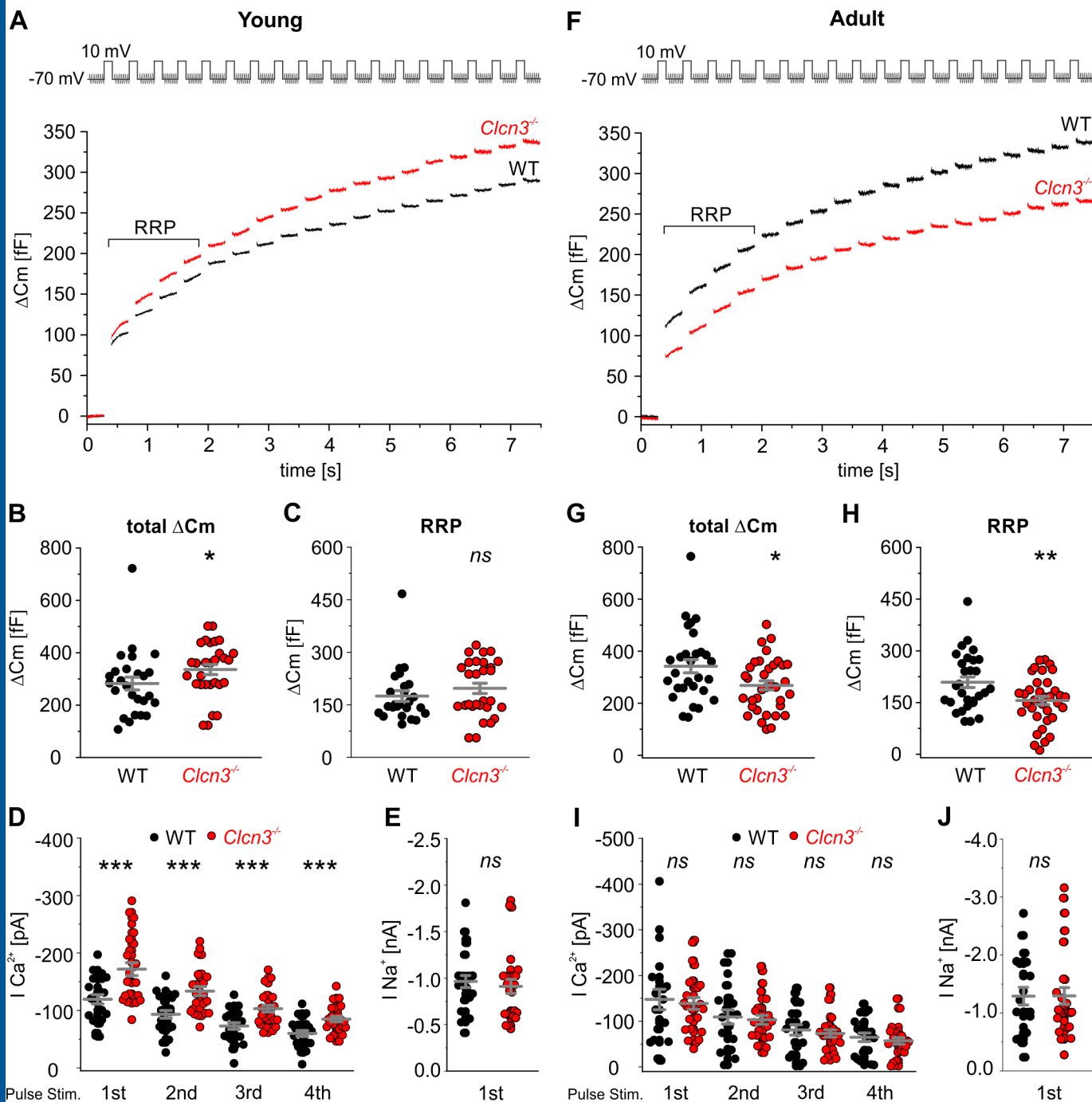
848 **Table 1. mRNA transcripts levels of CIC-3 and CIC-5 in mouse adrenal gland**

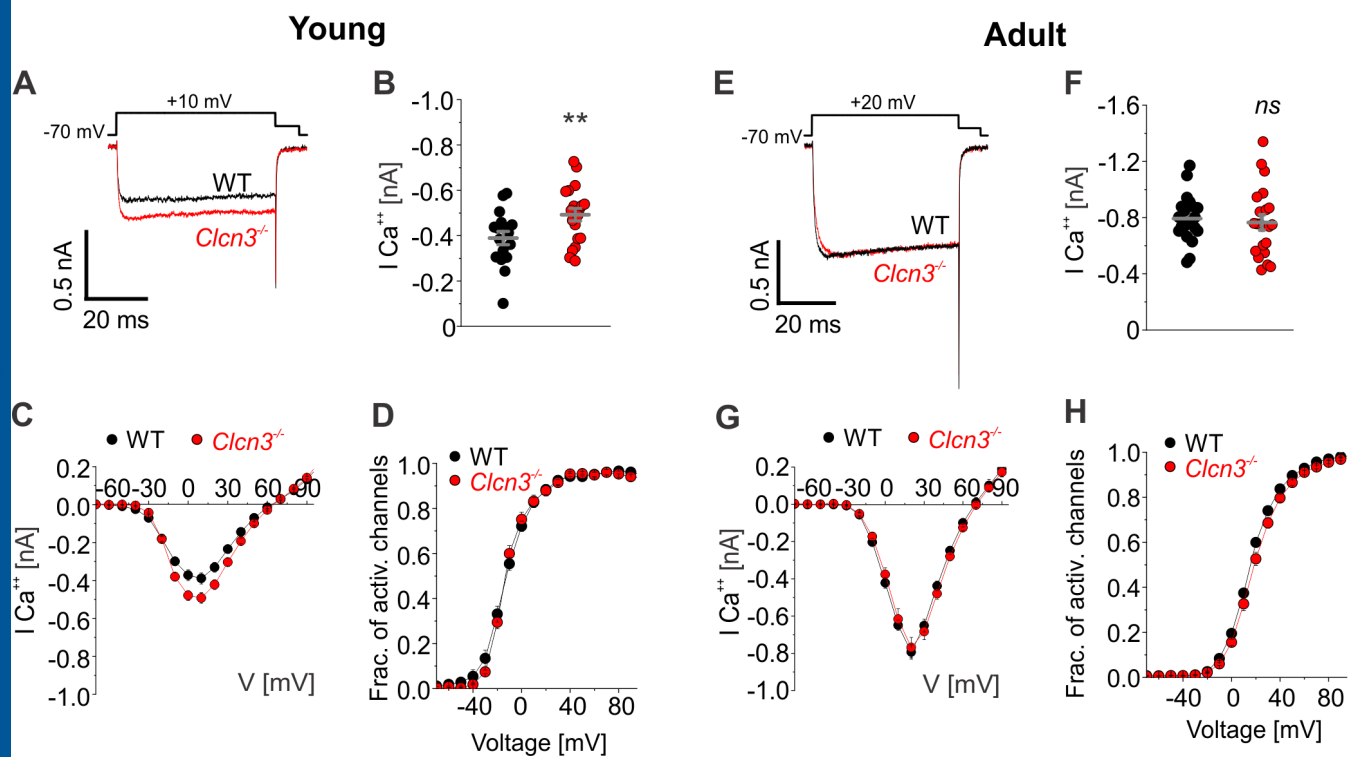
849 **Table 2. Properties of individual fusion events stimulated by extracellular application of high $[K^+]$**

850 **solution**

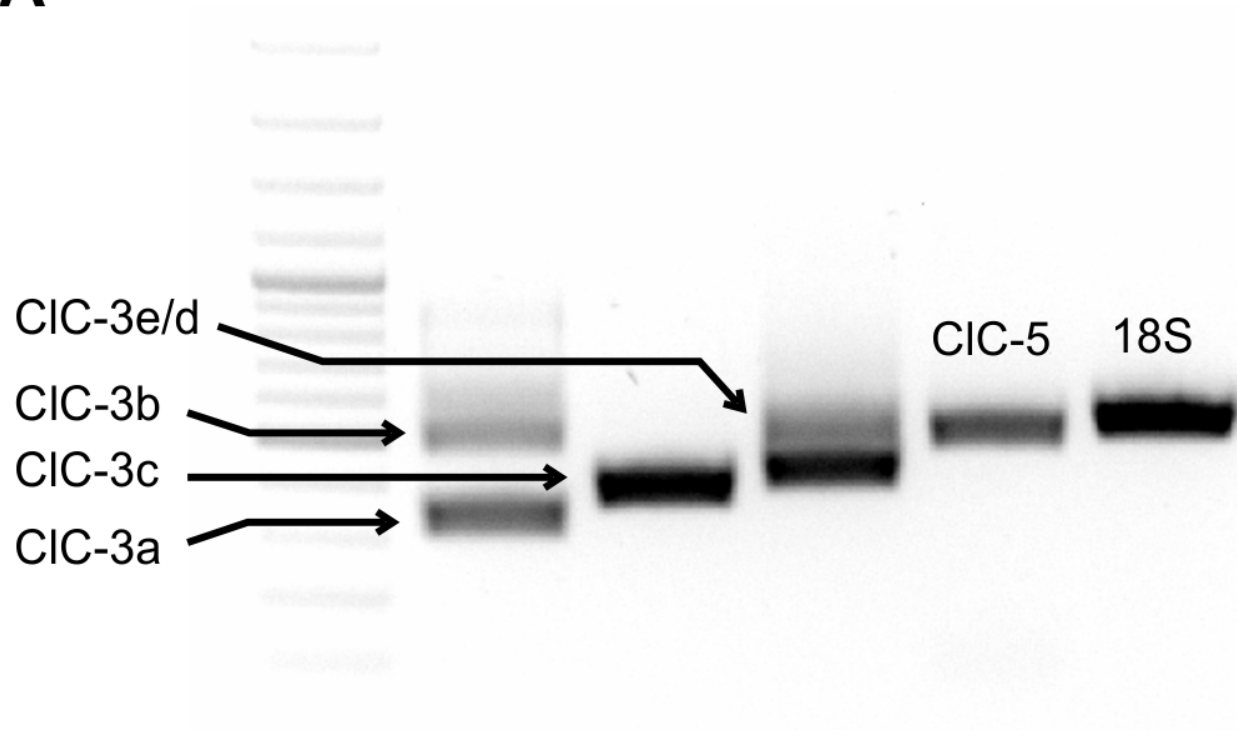
851 **Table 3. Properties of individual fusion events stimulated by intracellular perfusion of 3 μM free**

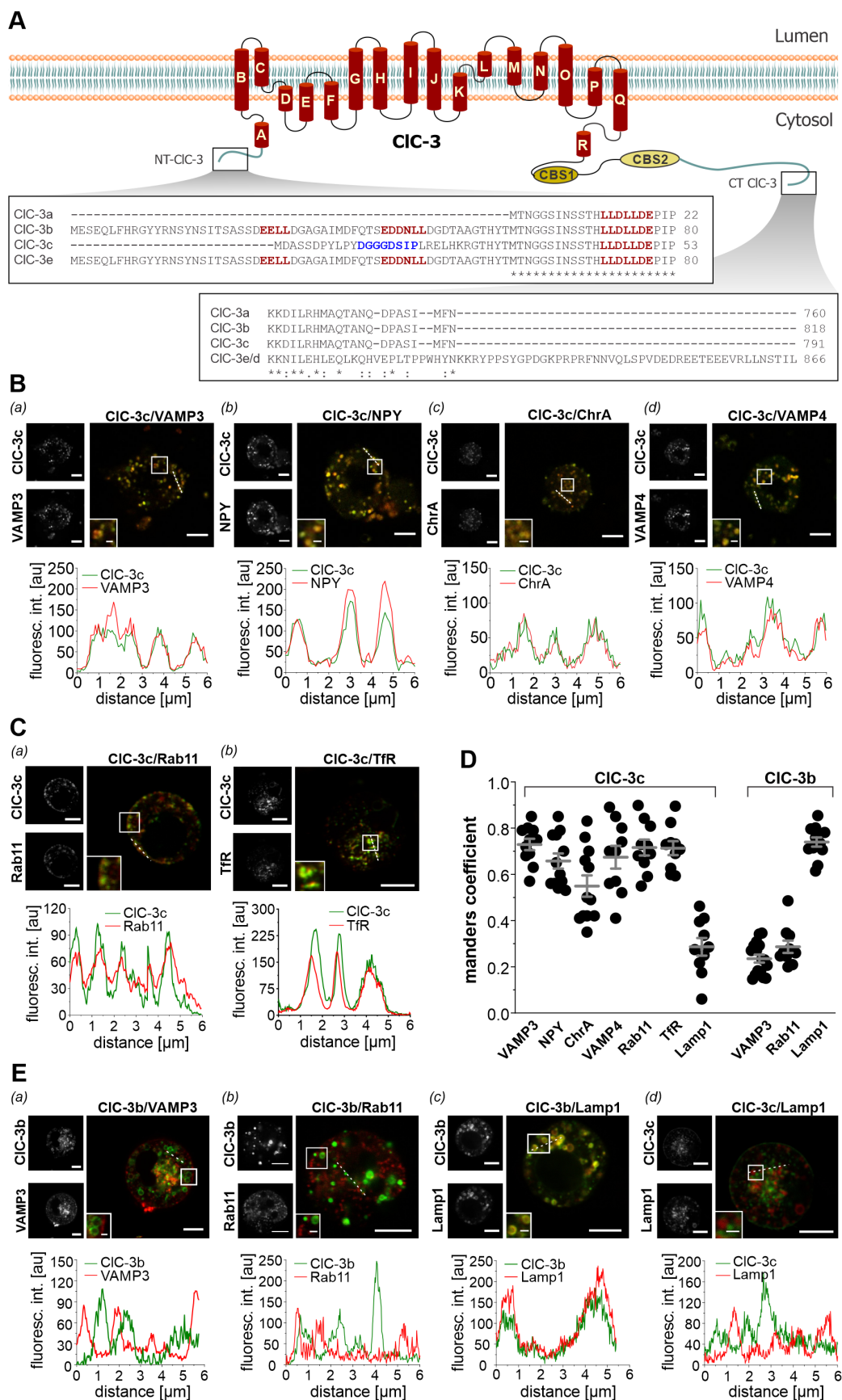
852 **Ca^{2+} solution**

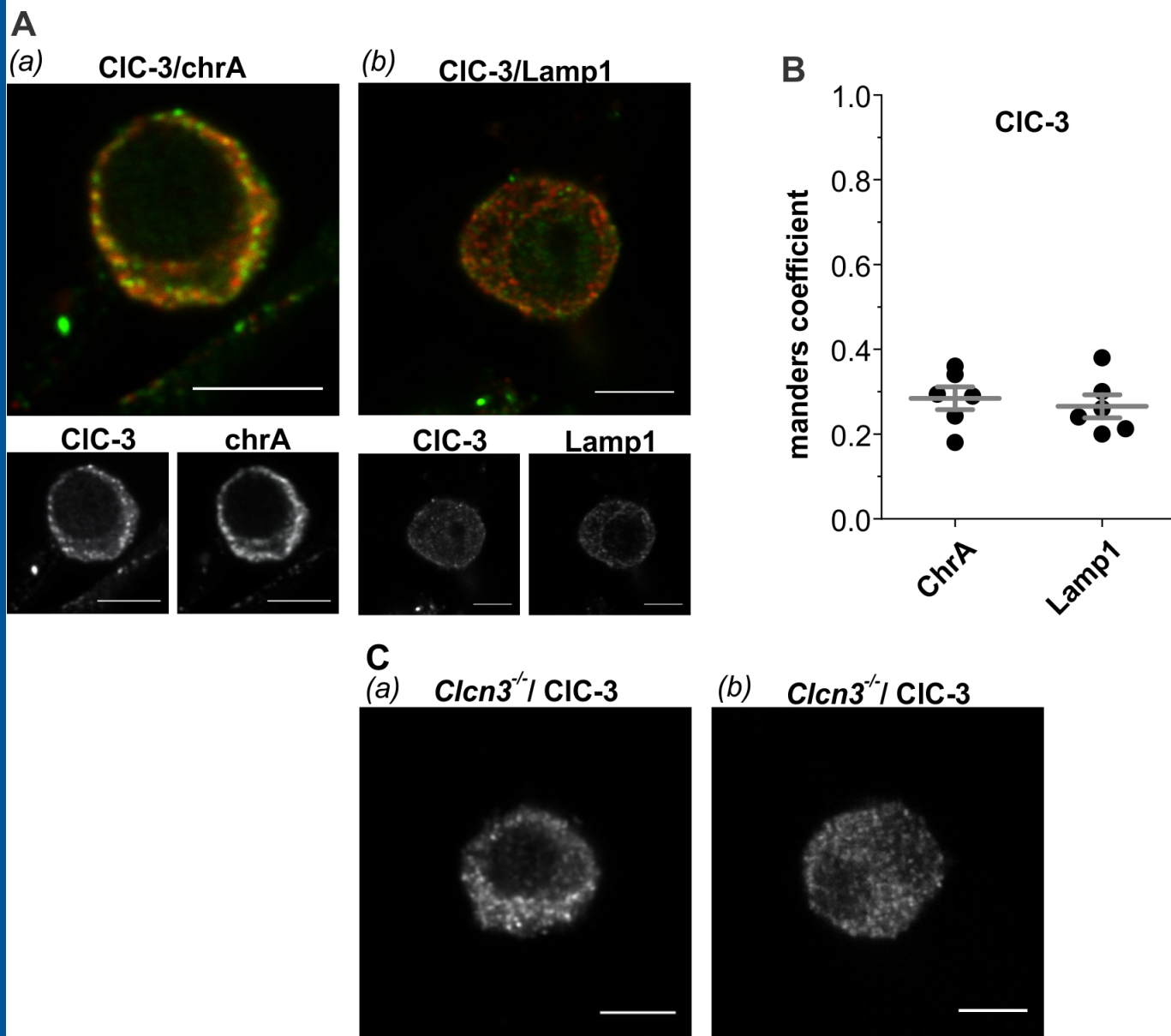


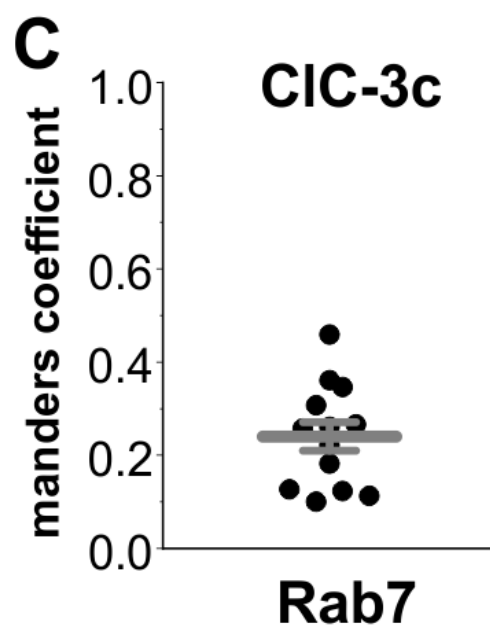
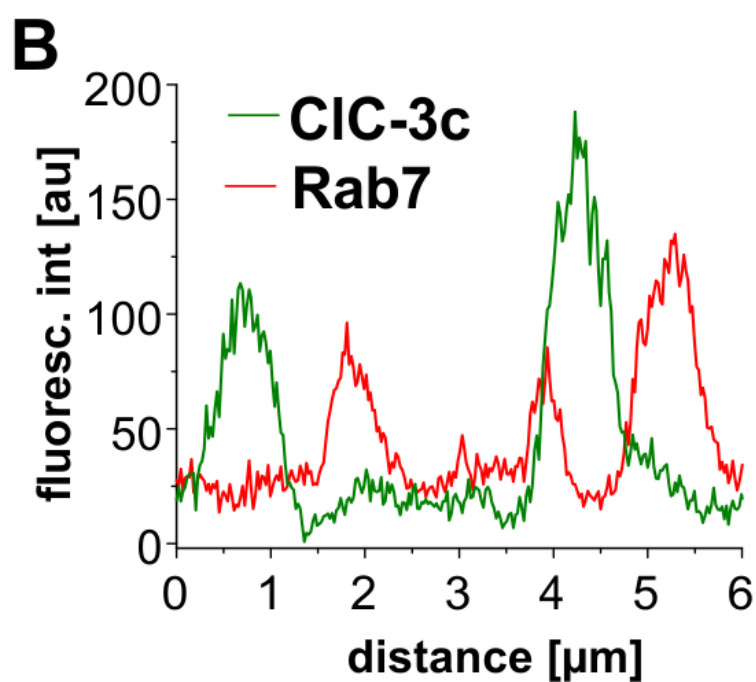
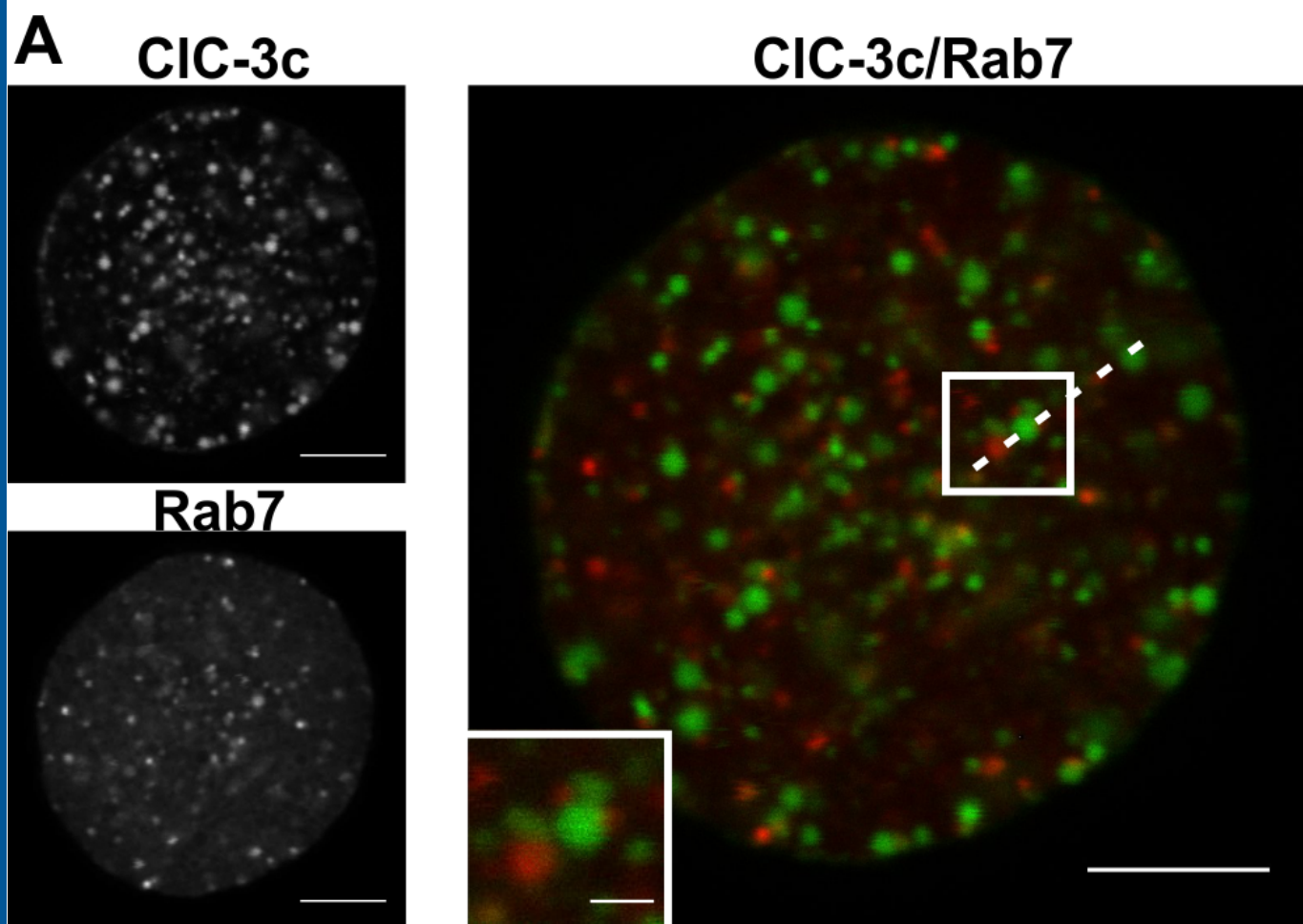


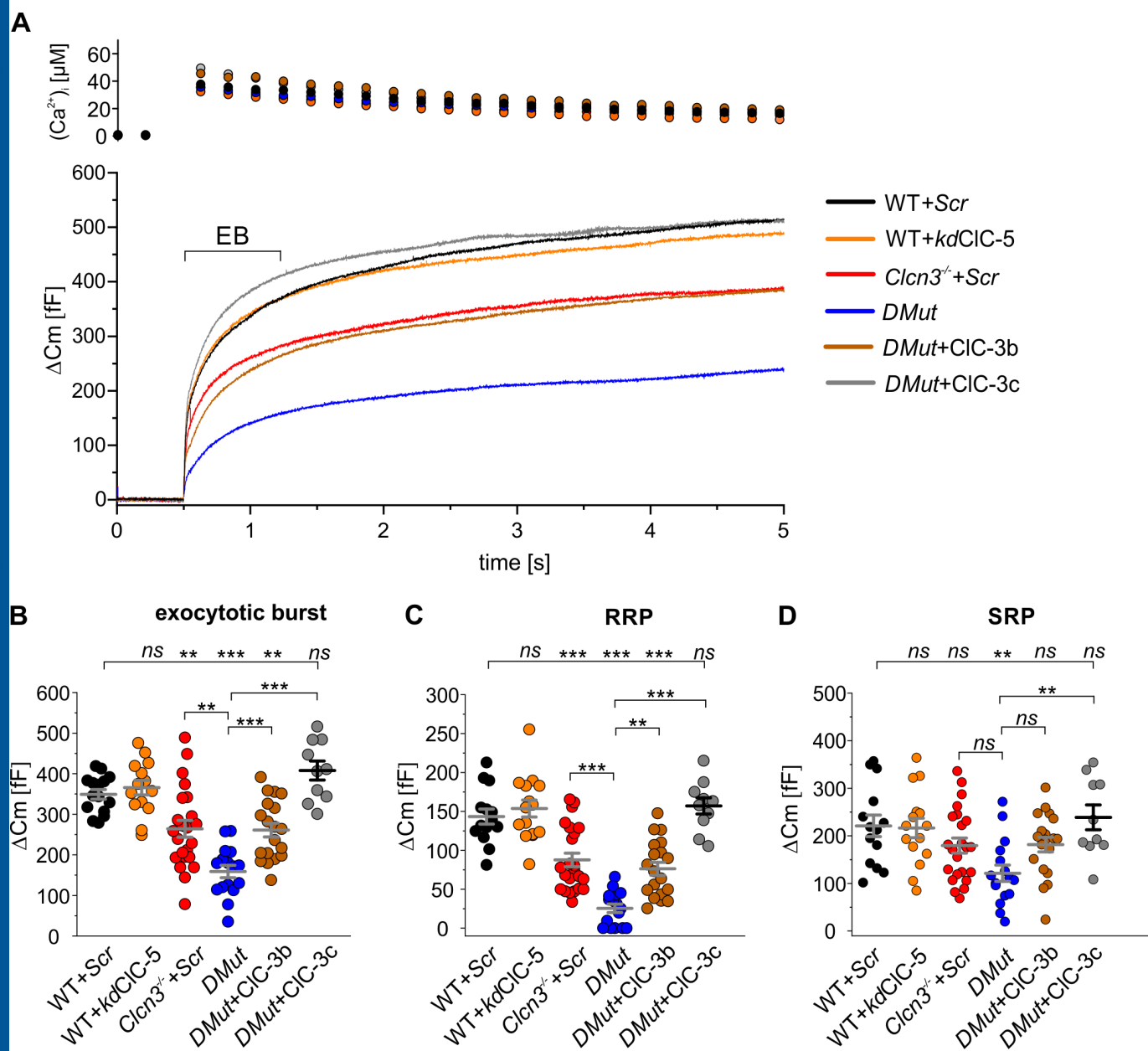
A

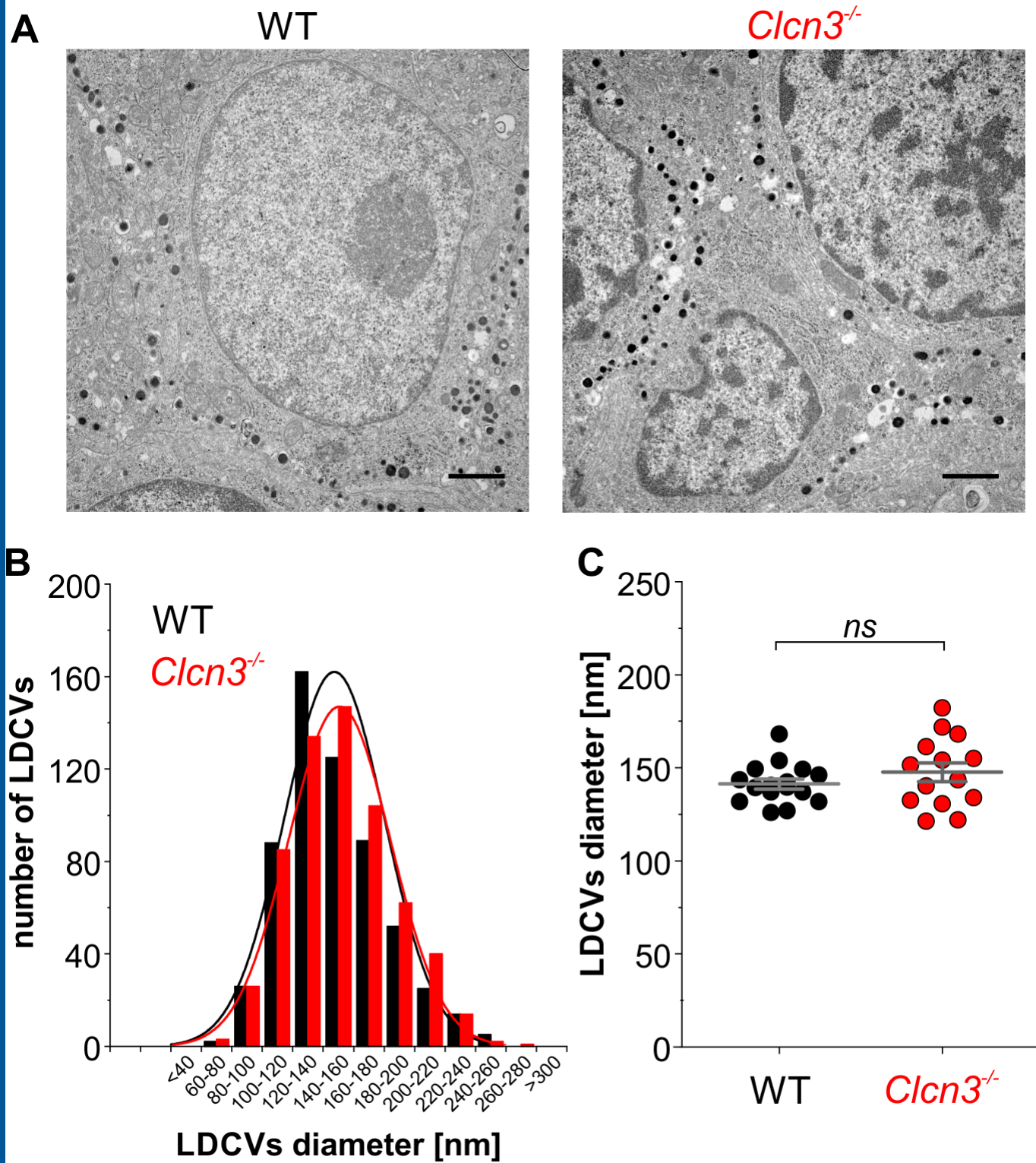


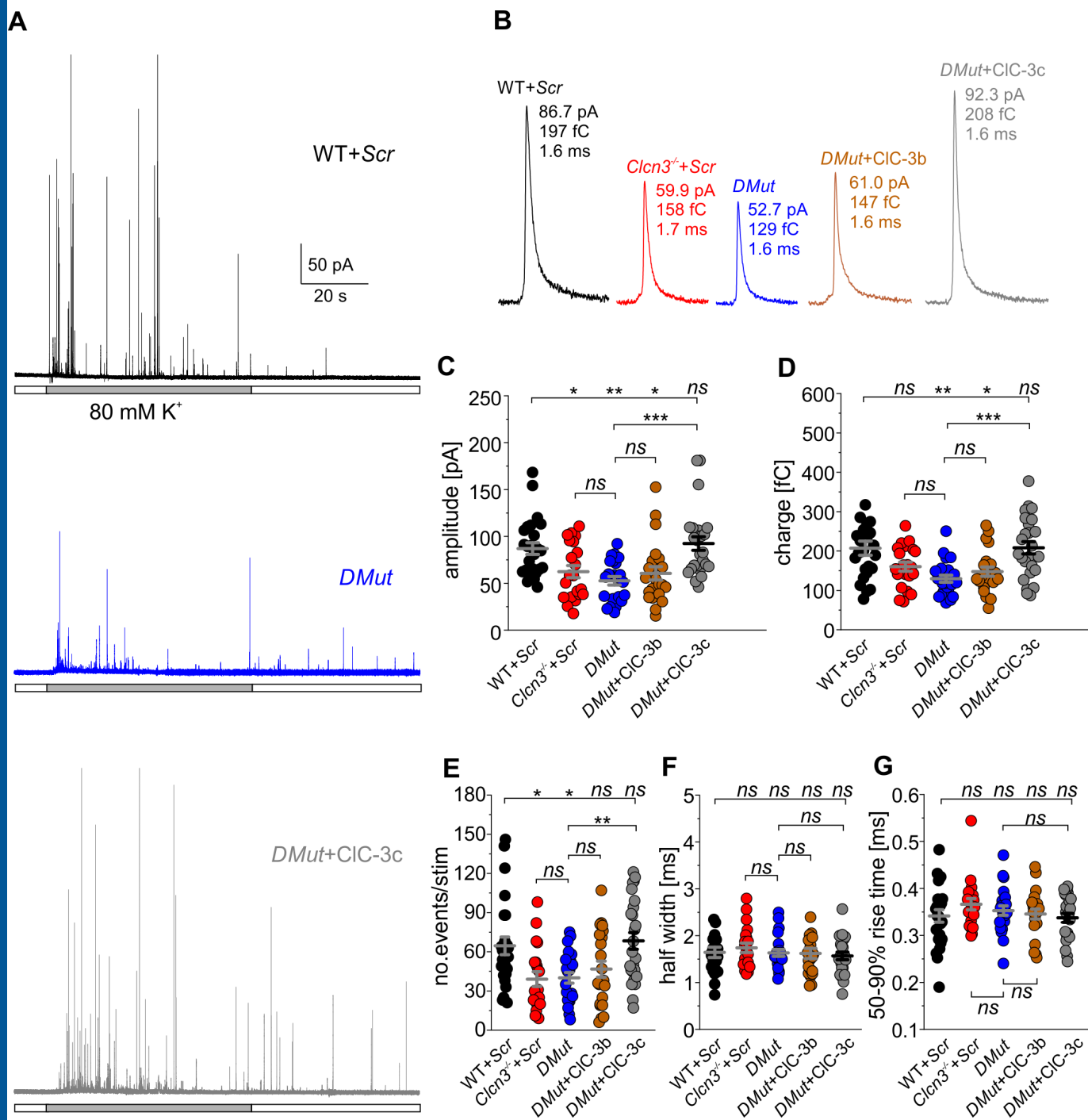


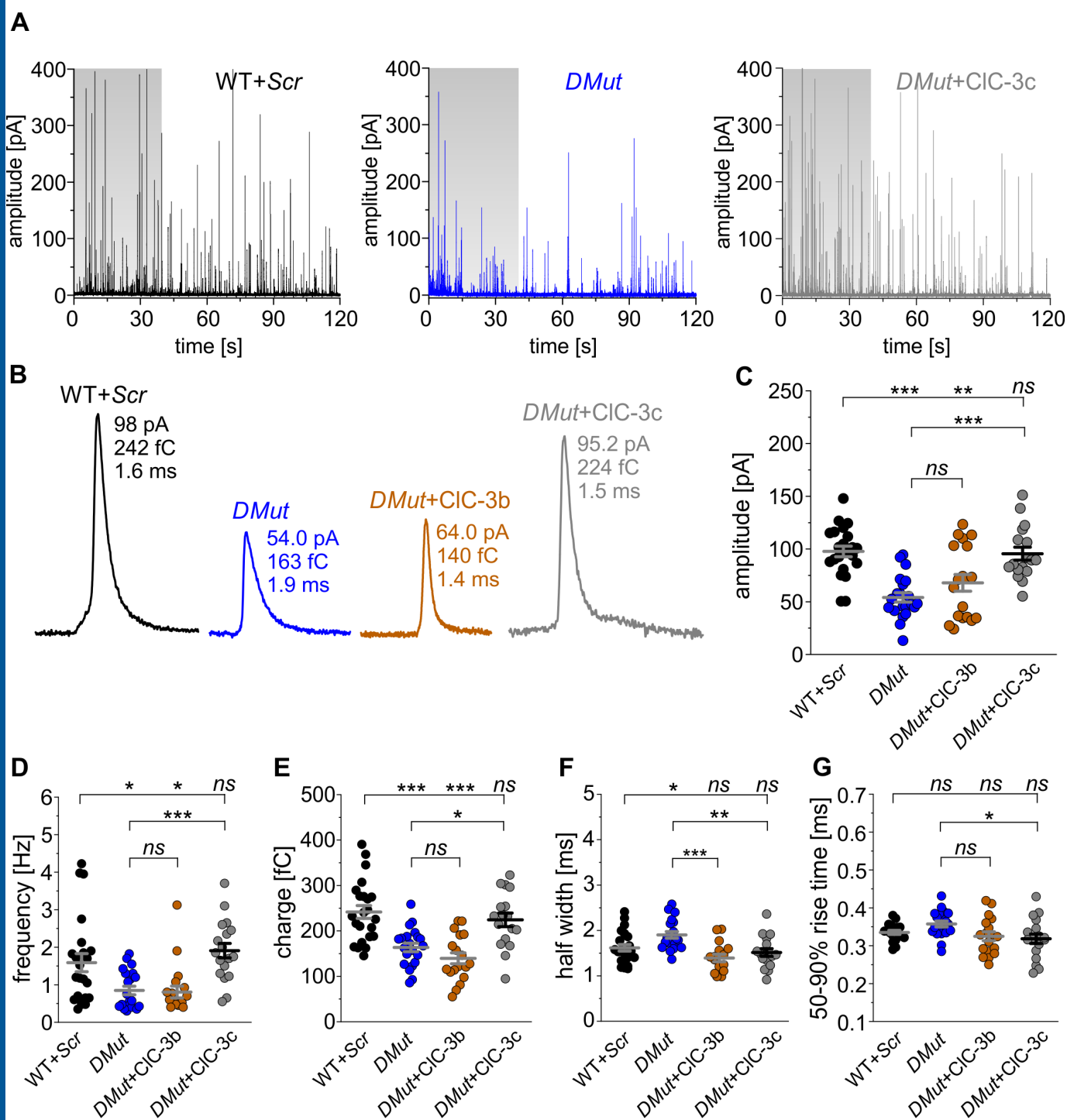


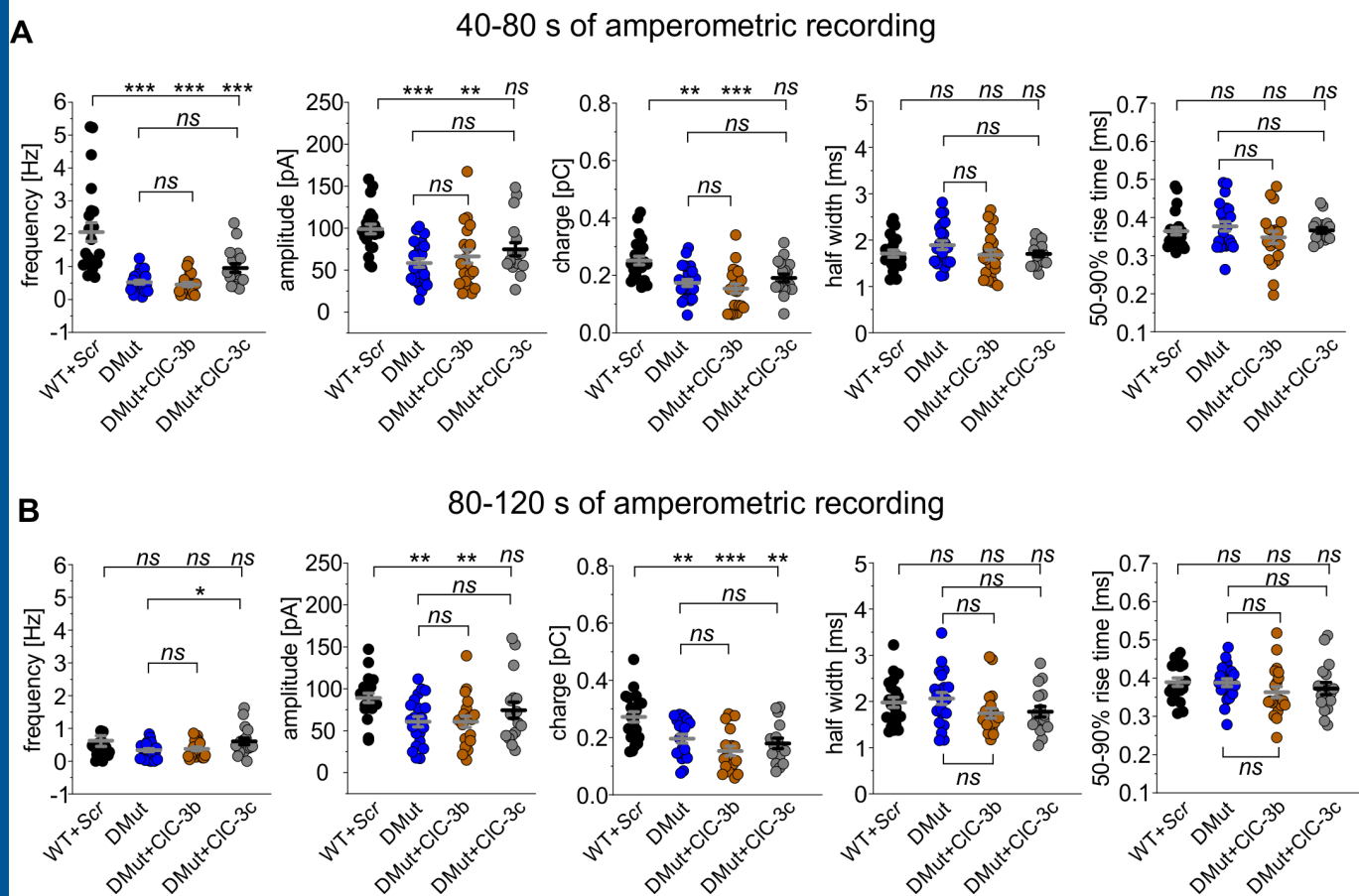


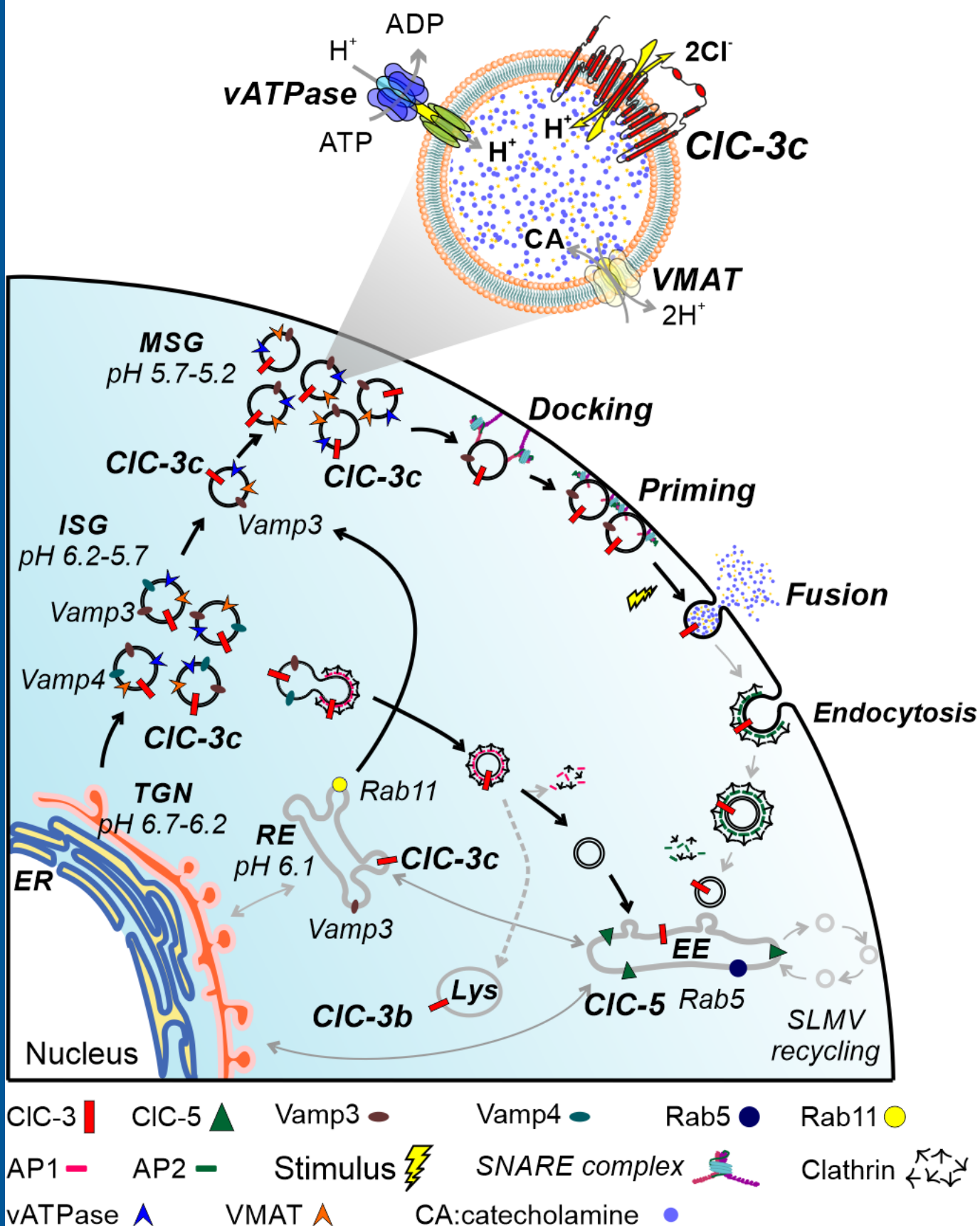












	Log [cDNA] 18S in WT	Log [cDNA] CIC-3 in WT	Log [cDNA] CIC-5 in WT	Log [cDNA] CIC-5 in <i>Clcn3</i> ^{-/-}
P0	6.80 ± 0.20	3.90 ± 0.05	2.70 ± 0.20	3.1 ± 0.15*, <i>p</i> = 0.02
P60	6.70 ± 0.40	3.80 ± 0.08	1.80 ± 0.20*, <i>p</i> = 0.02	

Table 1. mRNA transcripts levels of CIC-3 and CIC-5 in mouse adrenal gland. Adrenal glands were collected from C57BL/6 mouse strain at two different developmental stages, P0 (*n* = 5 mice) and P60 (*n* = 3) or *Clcn3*^{-/-} mice at P0 (*n* = 5). **p* < 0.05. Student's *t*-test. cDNA samples were measured in triplicate and are represented as mean ± s.e.m.

Genotype (No. of cells)	No. events/ stim.	Charge (pC)	Amplitude (pA)	50-90% Rise Time (ms)	Half-width (ms)	Foot parameters			
						% of events with foot	Foot amplitude (pA)	Foot duration (ms)	Foot charge (fC)
WT+Scr (n=24)	64.6±7.0	0.206±0.02	86.9± 6.2	0.34± 0.01	1.6± 0.1	41±2.5	5.3± 0.2	8.1±0.6	46.0±4.2
<i>Clcn3</i> ^{-/-} +Scr (n=20)	39.0± 5.6*	0.158±0.01*	59.9± 6.3*	0.37± 0.01 ^{ns}	1.7± 0.1 ^{ns}	43.7± 3.4 ^{ns}	4.7± 0.3 ^{ns}	8.6±0.8 ^{ns}	44.5±4.7 ^{ns}
<i>Dmut</i> (n=23)	40.0± 4.0*	0.129±0.009***	52.7± 4.5**	0.35± 0.01 ^{ns}	1.6± 0.1 ^{ns}	43± 3.4 ^{ns}	4.7± 0.3 ^{ns}	7.4±0.5 ^{ns}	36.7±3.8 ^{ns}
<i>DMut</i> +CIC-3b (n=21)	46.7± 6.1 ^{ns/} ^{ns}	0.147±0.011*/ ^{ns}	61.0± 7.4*/ ^{ns}	0.34± 0.01 ^{ns/} ^{ns}	1.6± 0.1 ^{ns/} ^{ns}	43.5± 3.9 ^{ns/} ^{ns}	4.8± 0.4 ^{ns/} ^{ns}	7.8±0.6 ^{ns/} ^{ns}	38.8±4.6 ^{ns/} ^{ns}
<i>DMut</i> +CIC-3c (n=25)	68.3±6.4 ^{ns/} ^{ns}	0.208±0.016 ^{ns/} ^{ns}	92.3±7.2 ^{ns/} ^{ns}	0.34± 0.01 ^{ns/} ^{ns}	1.6± 0.1 ^{ns/} ^{ns}	47.7±2.5 ^{ns/} ^{ns}	5.3± 0.3 ^{ns/} ^{ns}	9.2±0.5 ^{ns/} ^{ns}	46.6±3.8 ^{ns/} ^{ns}

Table 2. Properties of individual fusion events stimulated by extracellular application of high [K⁺] solution in WT or *Clcn3*^{-/-} chromaffin cells expressing scrambled/eGFP (WT+Scr or *Clcn3*^{-/-}+Scr) or *Clcn3*^{-/-} chromaffin cells expressing *kdCIC-5* (*DMut*) or *kdCIC-5*+CIC-3b (*DMut*+CIC-3b) or *kdCIC-5*+CIC-3c (*DMut*+CIC-3c). No. events/stim refer to the mean number of amperometric events obtained during the application of 80 mM potassium solution (60 s application). ****p*<0.001, ***p*<0.01, **p*<0.05, *ns* = not significant, versus WT+Scr and ****p*<0.001, ***p*<0.01, **p*<0.05, *ns* = not significant, versus *DMut*. One-way analysis of variance (Tukey's HSD post Hoc test). Data were collected from 5-7 independent experiments per condition and are represented as mean ± s.e.m.

Genotype (No. of cells/Total No. of events)	Event's frequency (Hz)	Charge (pC)	Amplitude (pA)	50-90% Rise Time (ms)	Half-width (ms)	Foot parameters			
						% of events with foot	Foot amplitude (pA)	Foot duration (ms)	Foot charge (fC)
WT+Scr (n=23/1462)	1.6±0.24	0.241±0.01	97.7±5.0	0.33±0.01	1.6±0.1	25.9±1.8	6.0±0.4	6.3±0.5	42.1±4.4
<i>Dmut</i> (n=20/801)	0.84±0.11*	0.163±0.009***	52.2±4.2***	0.35±0.01 ^{ns}	1.9±0.1*	23.8±2.2 ^{ns}	4.7±0.3 ^{ns}	5.5±0.3 ^{ns}	28.0±2.5*
<i>DMut+CIC-3b</i> (n=18/717)	0.8±0.1*/ ^{ns}	0.139±0.01***/ ^{ns}	64.8±7.7*/ ^{ns}	0.32±0.01 ^{ns}	1.4±0.1 ^{ns} */***	23.9±2.3 ^{ns} / ^{ns}	4.7±0.5 ^{ns} / ^{ns}	5.6±0.4 ^{ns} / ^{ns}	31.6±4.5 ^{ns} / ^{ns}
<i>DMut+CIC-3c</i> (n=17/1375)	1.9±0.19 ^{ns} */***	0.224±0.015 ^{ns} /*	95.8±6.1 ^{ns} /*	0.32±0.01 ^{ns} /*	1.5±0.1 ^{ns} /*	29.5±3.0 ^{ns} / ^{ns}	5.6±0.2 ^{ns} / ^{ns}	4.8±0.3 ^{ns} / ^{ns}	30.0±1.9 ^{ns} / ^{ns}

Table 3. Properties of individual fusion events stimulated by intracellular perfusion of 3μM free Ca²⁺ solution in WT chromaffin cells expressing scrambled/eGFP (WT+Scr) or *Clen3*^{-/-} chromaffin cells expressing *kdCIC-5* (*DMut*) or *kdCIC-5+CIC-3b* (*DMut+CIC-3b*) or *kdCIC-5+CIC-3c* (*DMut+CIC-3c*). “No. of cells/Total No. of events” denoted the number of cell and the total number of events analyzed per condition. Event's frequency was calculated over the first 40 s of amperometric recording. ****p*<0.001, ***p*<0.01, **p*<0.05, *ns* = not significant, versus WT+Scr and ****p*<0.001, ***p*<0.01, **p*<0.05, *ns* = not significant, versus *DMut*. One-way analysis of variance (Tukey's HSD post Hoc test). Data were collected from 4-5 independent experiments per condition and are represented as mean ± s.e.m.